Journal of
Medicinal Chemistry

Article

Systematic Variation of Pyrrolobenzodiazepine (PBD)-dimer Payload Physicochemical Properties Impacts Efficacy and Tolerability of the Corresponding Antibody-Drug Conjugates

Leanna R. Staben, Jinhua Chen, Josefa dela Cruz-Chuh, Geoffrey Del Rosario, Mary Ann Go, Jun Guo, Siamak Cyrus Khojasteh, Katherine R. Kozak, Guangmin Li, Carl Ng, Gail Lewis Phillips, Thomas H. Pillow, Rebecca K. Rowntree, John Wai, Binqing Wei, Keyang Xu, Zijin Xu, Shang-Fan Yu, Donglu Zhang, and Peter S. Dragovich

J. Med. Chem., **Just Accepted Manuscript** • DOI: 10.1021/acs.jmedchem.0c00691 • Publication Date (Web): 31 Jul 2020

Just Accepted

is published by the American Chemical Society. 1155 Sixteenth Street N.W., Washington, DC 20036

Systematic Variation of Pyrrolobenzodiazepine (PBD)-dimer Payload Physicochemical Properties Impacts Efficacy and Tolerability of the Corresponding Antibody-Drug Conjugates

Leanna R. Staben,[†] Jinhua Chen,[‡] Josefa dela Cruz-Chuh,[†] Geoff del Rosario,[†] Mary Ann Go,[†] Jun Guo,[†] S. Cyrus Khojasteh,[†] Katherine R. Kozak,[†] Guangmin Li,[†] Carl Ng,[†] Gail D. Lewis Phillips,[†] Thomas H. Pillow,[†] Rebecca K. Rowntree,[†] John Wai,[‡] BinQing Wei,[†] Keyang Xu,[†] Zijin Xu,[‡] Shang-Fan Yu,[†] Donglu Zhang,[†] Peter S. Dragovich*[,†]

[†]Genentech, Inc., 1 DNA Way, South San Francisco, California 94080, USA

[‡]WuXi AppTec Co., Ltd, 288 Fute Zhong Road, Waigaoqiao Free Trade Zone, Shanghai 200131, China.

RECEIVED DATE (to be automatically inserted after manuscript is accepted)

ABSTRACT: Cytotoxic pyrrolobenzodiazepine (PBD)-dimer molecules are frequently utilized as payloads for antibody-drug conjugates (ADCs), and many examples are currently in clinical development. In order to further explore this ADC payload class, the physicochemical properties of various PBD-dimer molecules were modified by the systematic introduction of acidic and basic moieties into their chemical structures. The impact of these changes on DNA binding, cell membrane permeability, and *in vitro* antiproliferation potency was respectively determined using a DNA alkylation assay, PAMPA assessments, and cell-based cytotoxicity measurements conducted with a variety of cancer lines. The modified PBD-dimer compounds were subsequently incorporated into CD22-targeting ADCs, and these entities were profiled in a variety of *in vitro* and *in vivo* experiments. Introduction of a strongly basic moiety into the PBD-dimer scaffold afforded a conjugate with dramatically worsened mouse tolerability properties relative to ADCs derived from related payloads which lacked the basic group.

INTRODUCTION

Pyrrolobenzodiazepine (PBD)-dimers are compounds which form covalent DNA interstrand cross-links in a sequence-dependent manner and which exhibit broad-spectrum sub-nanomolar antiproliferative activities against a variety of cancer cell lines.[1] Because of their exceptional cell potencies, PBD-dimers have been extensively employed as antibody-drug conjugate (ADC) payloads, and ADCs bearing such entities have been studied in advanced preclinical experiments and/or human clinical trials.[1] For example, SG2057 {(*11aS,11a'S*)-8,8'-(pentane-1,5-diylbis(oxy))bis(7-methoxy-2-methylene-1,2,3,11a-tetrahydro-5*H*-benzo[*e*]pyrrolo[1,2-*a*][1,4]diazepin-5-one), compound **1**} was incorporated into ADCs designed to treat acute myeloid leukemia (AML)[2] or HER2-expressing cancers[3] while SG3199 {(*11aS,11a'S*)-8,8'-(pentane-1,5-diylbis(oxy))bis(7-methoxy-2-methyl-1,11a-dihydro-5*H*-benzo[*e*]pyrrolo[1,2-*a*][1,4]diazepin-5-one), compound **2**} was employed as a component of rovalpituzumab tesirine ("Rova-T") which progressed to phase 3 clinical trials for the treatment of small-cell lung cancer.[4] In addition, SG1882 {(*S*)-2-(4-aminophenyl)-7-methoxy-8-(3-(((*S*)-7-methoxy-2-(4-methoxyphenyl)-5-oxo-5,11a-dihydro-1*H*-benzo[*e*]pyrrolo[1,2-*a*][1,4]diazepin-8-yl)oxy)-propoxy)-1,11a-dihydro-5*H*-benzo[*e*]pyrrolo[1,2-*a*][1,4]diazepin-5-one, compound **3**} was the cytotoxic payload associated with vadastuximab talirine which was assessed in phase 3 trials to treat acute myeloid leukemia (AML).[5] Several additional PBD-dimer-containing ADCs are currently undergoing clinical evaluation against a variety of cancers including loncastuximab tesirine (ADCT-402),[6] ADCT-601,[7] MEDI-2228,[8] and camidanlumab tesirine (ADCT-301).[9] In spite of these advancements, the late-stage clinical failures of both Rova-T[10] and vadastuximab talirine[11] suggest that additional optimization of the PBD-dimer entities may be required in order to fully realize the therapeutic potential of this ADC payload class.

Figure 1. Representative cytotoxic PBD-dimers employed as ADC payloads.

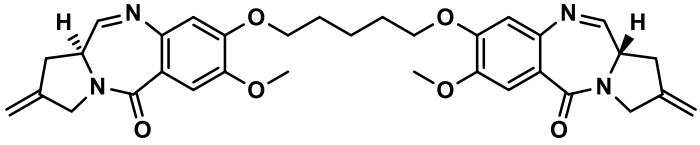

1 (SG2057)

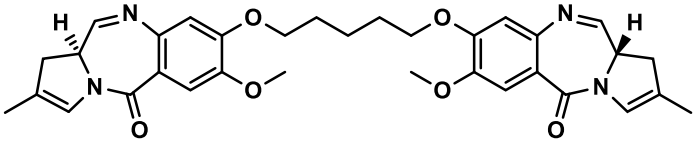

2 (SG3199)

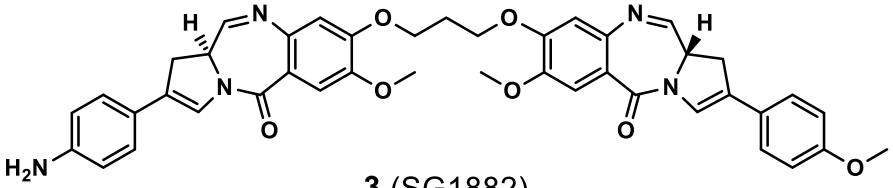

3 (SG1882)

As part of our own explorations of PBD-dimer-containing ADCs which also employed linkers that afforded lysosomal cleavage,[2,3] we wished to better understand how modifications to the physicochemical properties of the cytotoxic payloads impacted the *in vitro* and *in vivo* performance of the associated conjugates. In particular, we were curious to learn how the incorporation of acidic or basic moieties into the chemical structures of typical PBD-dimers might alter efficacy and/or tolerability outcomes associated with ADCs constructed from the

modified payloads. We also desired to understand how the results of these alterations compared to those associated with other well-known ADC payload classes. Prior studies of related ADC payload modifications include comparison of cell-permeable and cell-impermeable auristatin derivatives (MMAE and MMAF, respectively),[12] modification of maytansinoid-derived payload physicochemical properties,[13] and examination of topoisomerase inhibitor payloads with varying cell-permeability characteristics.[14] However, there are currently few published examples that study the impact of physicochemical property modification of the PBD-dimer ADC payload class.[15,16] In this report, we describe our efforts to systematically modify PBD-dimer physicochemical properties via the introduction of various ionizable functional groups as part of a focused effort to better understand such impacts. We also detail *in vitro* and *in vivo* testing results of antibody-drug conjugates derived from the new PBD-dimer entities which explore how these payload modifications alter ADC bioactivity in both *in vitro* and *in vivo* settings. In addition, we compare the physicochemical property effects observed for the modified PBD-dimers and associated conjugates with those previously reported for other ADC payload classes.[12-15]

RESULTS and DISCUSSION

We began our explorations by identifying a location within the PBD-dimer chemical structure that could be employed for the introduction of the desired diverse ionizable functionalities without significantly impacting the ability of the molecules to bind to the DNA minor groove and subsequently cross-link the nucleic acid.[17] We were inspired by our previous studies which examined ADCs constructed from non-cleavable linker-drugs bearing a centrally-

located phenyl moiety in the PBD-dimer structure (e.g., compound **4**, Figure 2).[18] Such ADCs were highly active in both *in vitro* and *in vivo* experiments, and these results indicated that the alkyne/PEG fragment, which would remain attached to the PBD-dimer core structure following lysosomal catabolism of the associated antibody, did not significantly impede DNA binding and/or alkylation by the cytotoxic compound. We therefore sought to utilize a related alkyne-based attachment strategy to derivatize the PBD-dimer core structure with the desired ionizable functional groups. Accordingly, we designed compounds **5-9** (Table 1) in which the various structural changes were incorporated at the terminus of the phenyl-alkyne moiety present in the center of the PBD-dimer molecules. As shown in Table 1, the functionalities employed in **5-9** were purposely selected to span a range of acidic and basic moieties with the methyl group present in **7** serving as a non-ionizable (neutral) comparator. In addition, the degree to which these acidic and basic groups ionized was expected to vary as the compounds transitioned between various biological environments as a result of their antibody-mediated intracellular delivery (e.g., compound **6** was anticipated to be predominantly ionized in the neutral cytosol but significantly less so in the weakly acidic lysosome). As part of these designs, we also envisioned subsequently connecting the new PBD-dimer entities to antibodies using well-precedented dipeptide-containing linkers that could be attached to the N-10 positions of the PBD structures (Table 1, Figure 2).

Figure 2. Alkyne-containing PBD-dimer linker-drug employed in our previous studies (ref. 18).

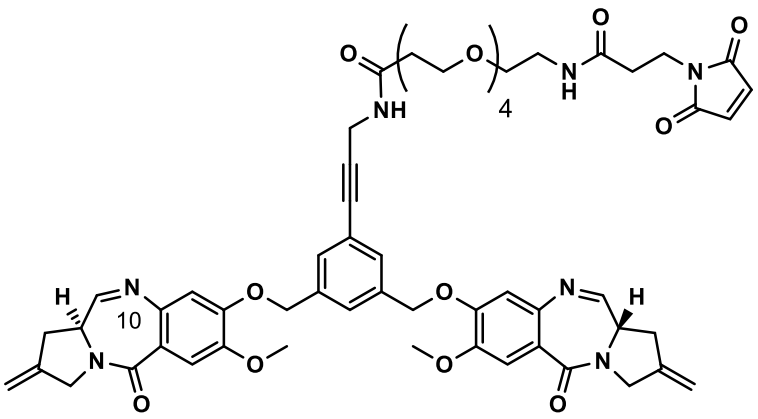

4

Table 1. Structures and physicochemical and biological properties of compounds **5-9**.

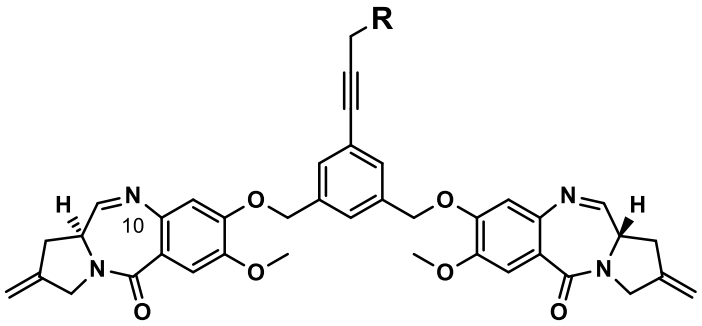

		Physico-Chem		DNA Alkylation (% remain, 1 h)[a]		PAMPA Pe ($x10^{-6}$ cm/s)[b]		Cell Antiproliferation IC_{50} (pM)[c]		
Cmpd.	R	Class	Calcd pKa[d]	Strand 1	Strand 2	pH = 4.0	pH = 7.4	BJAB	KPL4	Other Lines (Average)[e]
5	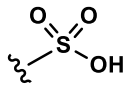	Strong Acid	1.5	62	58	0.68	0.60	>20,000	>20,000	>20,000 (n = 6)
6	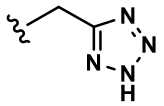	Weak Acid	5.5	0	0	10	0.70[f]	4,300	15,000	8,500 (n = 5)[g]
7		Neutral	NA	30	27	37	48	3.3	23	24 (n = 6)
8	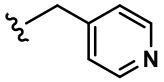	Weak Base	6.0[h]	30	30	2.4	36	8.6	65	108 (n = 7)
9	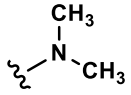	Strong Base	8.2[h]	0	0	0.34	2.0	29	86	264 (n = 6)
10	NA	NA	NA	100	100	68	61	5,000	72,000	ND
1	NA	NA	NA	4	0	15	11	14	53	67 (n = 7)

[a]Percent of unalkylated single-strand DNA remaining following independent exposure of double-strand DNA to 100 μM of each compound for 1 hour. 0 = strong alkylation observed, 100 = no (weak) alkylation observed. [b]PAMPA effective permeability determined for each compound at indicated pH; >20 = high, 10-20 = medium, <10 = low. [c]Antiproliferation activity determined in cell culture experiments using indicated cell line. Data are presented as geometric means (n = 4 per group); 95% confidence intervals are listed in Table S1. [d]pKa value of the R-group appended to each compound calculated using the MoKa software package (version 2.6.6). [e]Average of antiproliferation values determined for each compound using a panel of 5-7 cell lines. See Table S2 for more details. [f]pH = 6.2. [g]Value does not include two tested cell lines with IC_{50} outcomes >100,000 pM. [h]Conjugate acid. NA = not applicable. ND = not determined.

As was observed in our prior work,[18] modelling studies performed with **5**-**9** suggested that the alkyne fragments would protrude away from the DNA minor groove into solvent and thereby minimize the impact of the various terminal functional groups on the ability of the new molecules to bind to DNA (Figure 3). To confirm that this was indeed the case, we assessed the ability of each compound to alkylate a fragment of double stranded DNA that contained a sequence known to be efficiently recognized by this class of cytotoxic agents.[19] In this semi-quantitative assessment, the methyl-containing compound **7** exhibited DNA alkylation activity that was somewhat weaker than that exhibited by the reference compound **1** which lacked the centrally located phenyl-alkyne moiety (Table 1). This outcome likely reflects altered interactions of the two PBD-dimers with the double-stranded oligonucleotide that presumably result from the different linkers used to connect the PBD-monomer units.

We next compared the DNA alkylation properties of compounds **5**, **6**, **8**, and **9** to those of **7** to determine the impact of the various ionizable groups that resided in the former molecules. As shown in Table 1, the weakly-basic pyridine-containing compound **8** was equipotent with **7**, while the strongly basic **9** was more active (similar to reference compound **1**). In contrast, the strongly acidic molecule **5** was somewhat less active than **7**. These outcomes suggested that the

positioning of the strongly ionizable moieties present in **5** and **9** by the designed alkyne fragment did not completely eliminate electrostatic interactions between those entities and the negatively charged phosphate backbone of the test oligonucleotide. The weaker alkylation activity exhibited by compound **8** relative to **9** likely results from only minimal ionization of the pyridine moiety at the neutral pH of the assay as compared to the considerable protonation expected for the dimethylamino group. Somewhat surprisingly, the tetrazole-containing compound **6** displayed strong DNA alkylation properties that were analogous to those exhibited by reference compound **1**. The origin of this activity is not known at this time, but may involve interaction of the (presumably ionized) tetrazole moiety with the test oligonucleotide and/or its associated water network in a manner that somehow compensates for the anticipated unfavorable electrostatic interactions with the DNA phosphates.

An important caveat associated with the above assessments is that a single fragment of test DNA was used to compare the molecules, and this fragment may not perfectly represent all nucleic acid sequences that are expected to be targeted by the molecules in cells. The semi-quantitative nature of the alkylation assay employed also adds some uncertainty to the described comparisons. In spite of these limitations, the DNA-binding assessments indicated that compounds **5**-**9** all retained measurable DNA alkylation properties that were considerably differentiated from a minor groove binding reference compound that was incapable of covalently modifying the nucleic acid (compound **10**, Figure 4, Table 1). For this reason, we chose to continue with the assessment of **5**-**9** as ADC payloads and the associated biological data will be reported later in this work. However, although we attempted to normalize DNA affinity among the new PBD-dimer molecules via the above assessments, this variable may still partially

contribute to the *in vitro* and *in vivo* outcomes described for the associated compounds and conjugates (see below for specific instances where this situation may apply).

Figure 3. Composite model of compounds **5-9** binding to the DNA minor groove. Pink atom indicates location of ionizable groups attached to terminus of central phenyl-alkyne moiety.

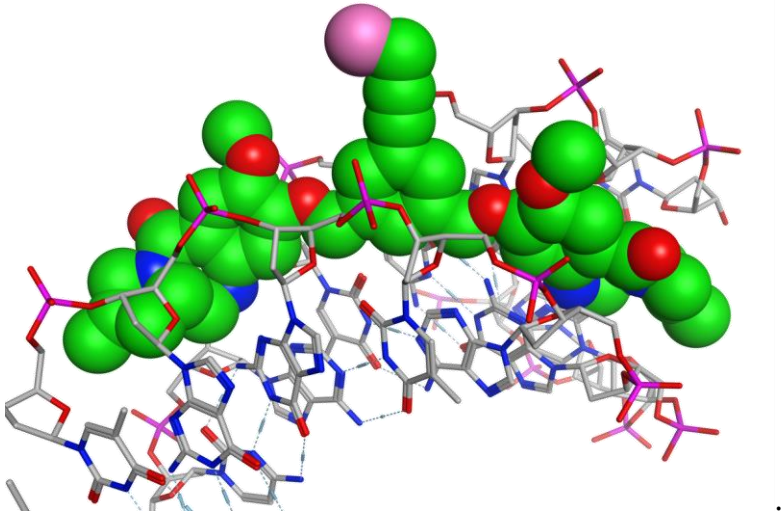

Figure 4. Reference compound **10** employed in DNA alkylation assessments as inactive control.

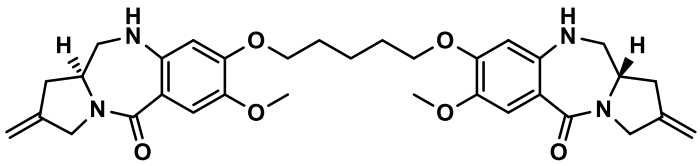

10

We expected the ionizable groups present in compounds **5**, **6**, **8**, and **9** to impact their cell membrane permeability relative to the non-ionizable methyl fragment incorporated into compound **7**. Given the nature and diversity of the ionizable moieties, we also expected the pH of the assay media to influence the outcomes. Accordingly, we employed PAMPA testing[20] as a surrogate for cell membrane permeability and assessed the new molecules at two different pH values. The first value (pH 4.0) was selected to mimic the lysosomal environment that the molecules were expected to encounter shortly after their release from a catabolized antibody-drug conjugate. The second value (pH 7.4) was intended to duplicate the cellular cytosol as well as the extracellular environment. As shown in Table 1, the measured PAMPA Pe parameters correlated well with the calculated pKa data for the various compounds at both pH values tested. In particular, the strongly acidic **5** exhibited low PAMPA Pe outcomes relative to neutral compound **7** at both pH 4.0 and 7.4. In contrast, the weakly acidic **6** displayed a much larger Pe at the former pH compared to the latter value that was consistent with its reduced ionization under the more acidic conditions. PAMPA results for the two basic molecules **8** and **9** were also predictably influenced by the pH employed in the assessments with both compounds exhibiting smaller Pe values at the more acidic pH relative to neutral conditions. Collectively, the PAMPA data indicated that PBD-dimers **5**-**9** might exhibit differing permeabilities toward biological membranes and that such differences would likely be dependent on the pH of the associated biological environment.

We next assessed the ability of compounds **5**-**9** to exhibit antiproliferation effects in *in vitro* cell-based experiments. This testing was conducted at near-neutral pH (7.4), and two diverse cell lines were employed: the B-cell-derived BJAB line and the KPL4 breast cancer line. As shown in Table 1, compound **5**, which contained the most acidic functional group and which

displayed the lowest PAMPA Pe values, was not active in the cell-based assessments when tested to relatively high concentrations (20 nM). In stark contrast, the neutral molecule **7** exhibited picomolar antiproliferation effects in both cell lines that were similar to those displayed by the well-characterized control compound **1** (Table 1). These data suggested that, as a result of sulfonic acid ionization at physiological pH, compound **5** was not able to effectively transition through the outer membranes of either employed cell line (differences in DNA binding/alkylation between **5** and **7** may also have contributed somewhat to the observed outcomes). The weakly acidic **6** also exhibited significantly impaired activity in these cell assays relative to compound **7** but was surprisingly more active than compound **5** in spite of a similarly low pH 7.4 PAMPA Pe value. The improved DNA alkylation properties of **6** relative to **5** may have contributed to the latter outcome. In contrast, the molecules bearing basic functional groups (**8** and **9**) displayed only slightly attenuated antiproliferation potencies relative to **7** (Table 1). The latter results were consistent with both **8** and **9** exhibiting PAMPA values at pH 7.4 that were predictive of good or moderate membrane permeability characteristics. In addition, the stronger DNA alkylation properties of **9** as compared to **7** may have helped compensate for the lower pH 7.4 PAMPA Pe value (and presumed poorer cell membrane permeability) displayed by the former molecule. Reassuringly, the BJAB and KPL4 outcomes also paralleled antiproliferation results obtained by testing compounds **5**-**9** against panels of five, six, or seven additional diverse cancer cell lines (Table 1 and Supporting Information).

Having profiled the new PBD-dimer compounds in the various *in vitro* assessments described above in unconjugated form, we sought to attach them to antibodies to further characterize their biological properties. Accordingly, we prepared CD22-targeting antibody conjugates **11a**-**15a** and the corresponding HER2 ADCs **11b**-**15b** (Table 2). The well-known

Valine-Citrulline (Val-Cit) protease-cleavable dipeptide trigger was incorporated into the design of these conjugates, and the PBD-dimer payloads were connected to this moiety via an N10 carbamate functional group and a para-amino-benzyloxy (PAB) self-immolative spacer.[21,22] ADCs bearing related PBD-dimer payloads that were linked to the antibodies via similar N10 carbamates displayed strong antigen-dependent anticancer activity in both *in vitro* and *in vivo* assessments.[4,22] These prior outcomes suggested that efficient delivery of the associated PBD-dimer payloads occurred following treatment of cells and tumors with the conjugates, and we were therefore confident that equally favorable delivery outcomes would occur with the new molecules under study. In addition, the new conjugates **11a**-**15a** and **11b**-**15b** were constructed via maleimide derivatization of cysteine residues that were engineered into the LC-K149 location of the antibody structures [drug-antibody ratios (DARs) of ~2.0].[23] This location and connection approach were known from our prior studies to afford conjugates that exhibited highly favorable *in vitro* and *in vivo* stability properties.[24] Significant retro-Michael-related deconjugation was therefore not expected to be observed with the new ADCs. In addition, the CD22 antigen was known to be highly expressed on BJAB cells,[25] and conjugates which target this entity had previously shown strong *in vitro* and *in vivo* biological activities.[26] Similarly, HER2 was well-precedented as an ADC target, and the antigen was highly expressed on KPL4 breast cancer cells (IHC 3+).[27] Conversely, the CD22 antigen was not highly expressed on KPL4 cells and the HER2 receptor was not significantly present on the surface of B-cell lines (e.g., BJAB). These differential expression patterns enabled the CD22 and HER2 conjugates to serve as respective negative (i.e., non-targeted) controls for KPL4 and B-cell ADC experiments.

Table 2. Structures and biological properties of conjugates **11a-15a** and **11b-15b**.

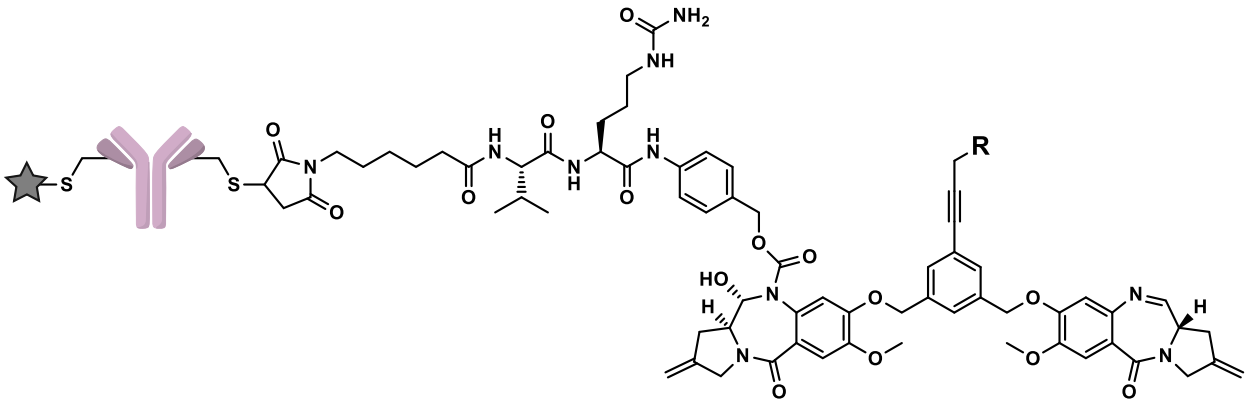

						Cell Antiproliferation IC_{50} (ng/mL)[c]			
R	Class	Calcd pKa[a]	ADC	Antigen	DAR[b]	BJAB (CD22)	WSU-DLCL2 (CD22)	KPL4 (HER2)	Jurkat (neg. control)
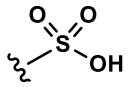	Strong Acid	1.5	**11a**	CD22	2.0	12	5.4	>10,000	>20,000
			11b	HER2	2.0	>20,000	>20,000	6.2	>20,000
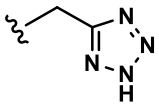	Weak Acid	5.5	**12a**	CD22	1.9	67[d]	14[d]	>1,000	15,000
			12b	HER2	1.8	>20,000	>20,000	0.54	>20,000
	Neutral	NA	**13a**	CD22	2.0	6.4	1.6	>1,000	450
			13b	HER2	2.0	2,200	560	0.68	820
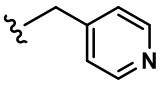	Weak Base	6.0[e]	**14a**	CD22	2.0	5.4	2.2	>10,000	1,900
			14b	HER2	2.0	4,200	2,500	0.51	1,900
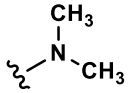	Strong Base	8.2[e]	**15a**	CD22	1.9	4.2	1.9	>700	1,600
			15b	HER2	2.0	1,300	870	0.27	810
Control 1[f]	NA	NA	**16a**	CD22[g]	1.7	14	7.1	ND	290
Control 2[f]	NA	NA	**16b**	HER2[g]	1.6	ND	ND	4.5	ND

[a]pKa value of the R-group appended to each PBD-dimer payload calculated using the MoKa software package (version 2.6.6). [b]Drug-antibody ratio. [c]Antiproliferation activity determined in cell culture experiments using indicated cell line. As these assessments were not all simultaneously performed, an appropriate control conjugate (**16a** or **16b**) was included in every determination to serve as an activity benchmark. Data are presented as geometric means (n = 4 per group); 95% confidence intervals are listed in Table S3. The targeted antigen expressed by each cell line (CD22 or HER2) is listed at the top of each column. [d]Control ADC (**16a**) IC_{50} was weaker than typically observed (BJAB = 74 ng/mL; WSU-DLCL2 = 20 ng/mL). [e]Conjugate acid. [f]Control ADC which releases compound **1** PBD-dimer payload (see Figure 6). [g]LC-V205 antibody attachment site; the alternate attachment site is not anticipated to impact *in vitro* potency relative to the LC-K149 site. NA = not applicable. ND = not determined. Star symbol = second copy of attached linker drug.

As shown in Table 2 and Figure 5, all of the CD22-targeting conjugates **11a**-**15a** exhibited strong antiproliferation activities when tested against the BJAB cell line that were similar to the potency displayed by a control conjugate which incorporated the well-known PBD-dimer **1** (**16a**, Figure 6). In contrast, the corresponding HER2 conjugates **11b**-**15b** afforded drastically weaker outcomes in the BJAB assessments (Table 2, Figure 5). These results were consistent with antigen-selective delivery of the new PBD-dimer payloads to the BJAB cells via the CD22-targeting ADCs. Related antiproliferation outcomes were also observed when the conjugates were tested against a second B-cell-derived and CD22-expressing cell line (WSU-DLCL2, Table 2, Figure 5; see Figure S1 for CD22 expression in WSU-DLCL2 cells). The near-equal activity of ADCs **11a**-**15a** against the B-cell lines was notable given the disparate antiproliferation potencies of the unconjugated PBD-dimer payloads depicted in Table 1 above (see Figure 7 as well). The strong activities of conjugates **11a** and **12a** against the BJAB line were particularly striking in light of the dramatically attenuated potencies observed for the corresponding unconjugated payloads against the same cell line (Tables 1 and 2, Figure 7). The described results paralleled those reported earlier for the auristatin-derived, acid-containing ADC

payload MMAF which is a relatively weak *in vitro* antiproliferative agent in unconjugated form but which exhibits significantly more potent cell-based activity when appropriately conjugated to an antibody.[12a] Note that **12a** exhibited anti-BJAB activity that was similar to control conjugate **16a** when both conjugates were tested side-by-side in the same antiproliferation assessment (Table 1). Thus, when normalized based on the activity of control compound **1**, **12a** is believed to be approximately equipotent with **11a** and **13a**-**15a** against the B-cell lines.

Figure 5. *In vitro* antiproliferation activities of PBD-dimer conjugates as a function of cell line.[a]

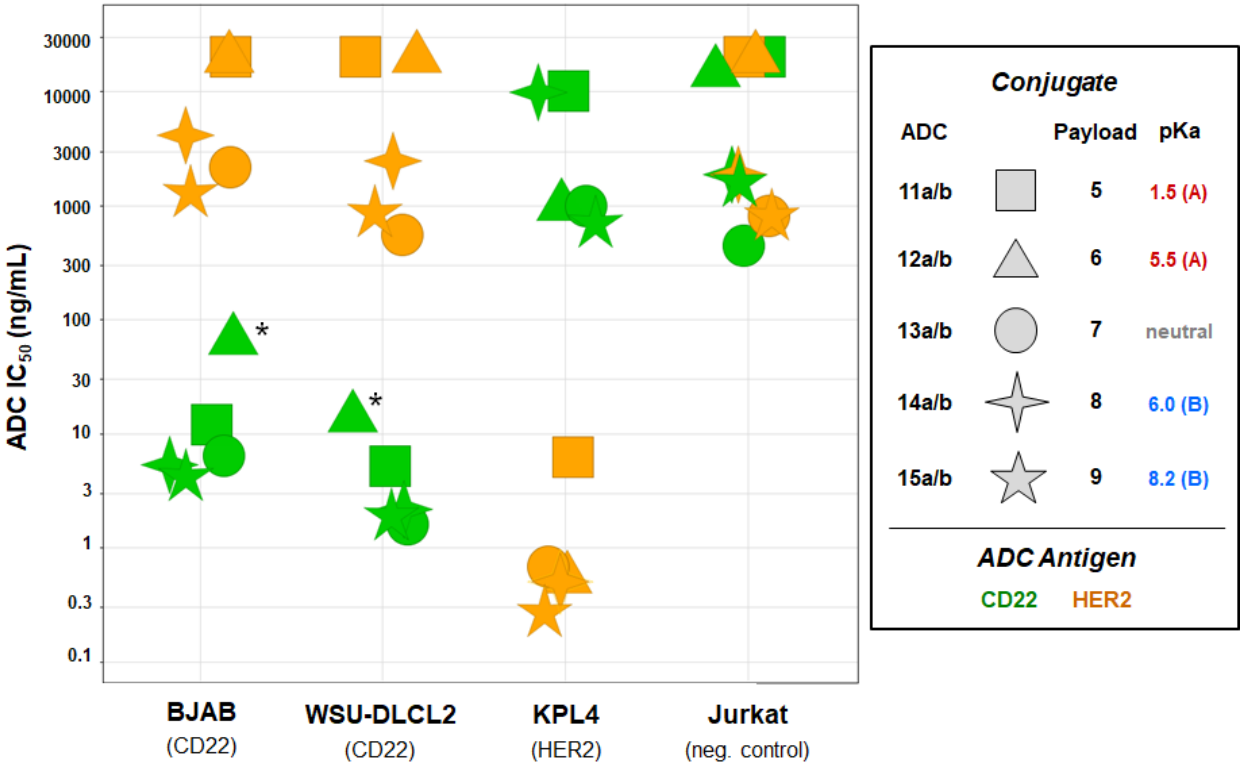

[a]Antiproliferation data are taken from Table 2. The targeted antigen expressed by each cell line (CD22 or HER2) is listed below each name. pKa values refer to the R-group appended to each PBD-dimer payload and were calculated using the MoKa software package (version 2.6.6); **red** = acidic, **blue** = basic (conjugate acid). *Control ADC (**16a**) IC_{50} was weaker than typically observed; see Table 2 for additional details.

Figure 6. Structure of control conjugates **16a** (CD22) and **16b** (HER2). Star symbol = second copy of attached linker drug.

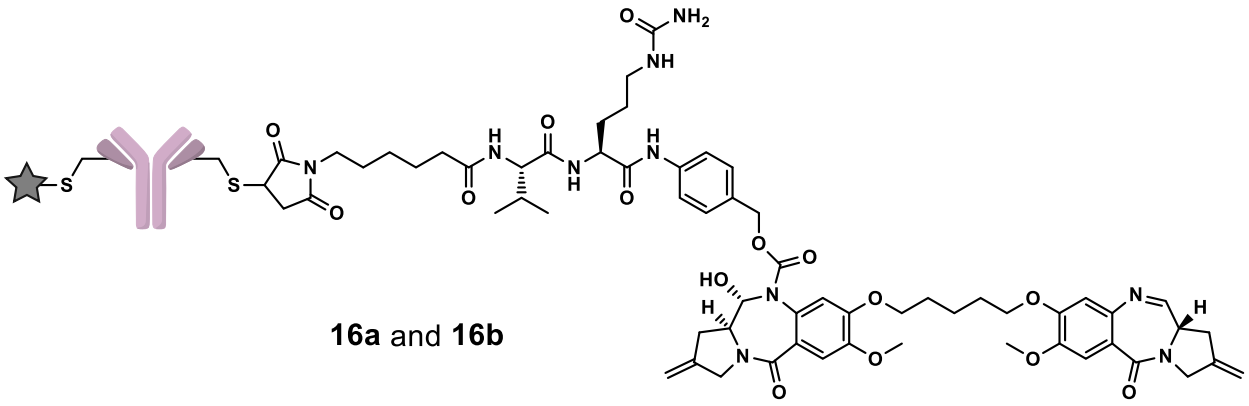

These results suggested that the PBD-dimer payloads containing acidic functional groups (including highly ionizable moieties such as the sulfonic acid present in **5**) were able to efficiently transition from the cellular lysosome to the cytosol and/or nucleus following antibody-mediated delivery. In the case of **5**, this transition occurred in spite of the payload exhibiting a low PAMPA Pe value at lysosomal pH that was suggestive of poor membrane permeability (Table 1). The origin of the potent *in vitro* antiproliferation activity of conjugates **11a** and **12a** is not known with certainty at this time. Some possibilities include (1) active transport of the released payloads across the lysosomal membrane,[28] (2) the lysosomal membrane being a more porous barrier with respect to small-molecule passive permeability

relative to the outer cell membrane, and (3) underestimation of payload membrane permeability properties via the PAMPA assessment. Additional experiments are thus required to further define the precise mechanism(s) by which these modified PBD-dimer ADC payloads exert their *in vitro* biological activities.

Figure 7. BJAB or KPL4 *in vitro* antiproliferation activities of PBD-dimer conjugates as a function of free payload *in vitro* antiproliferation potency.[a]

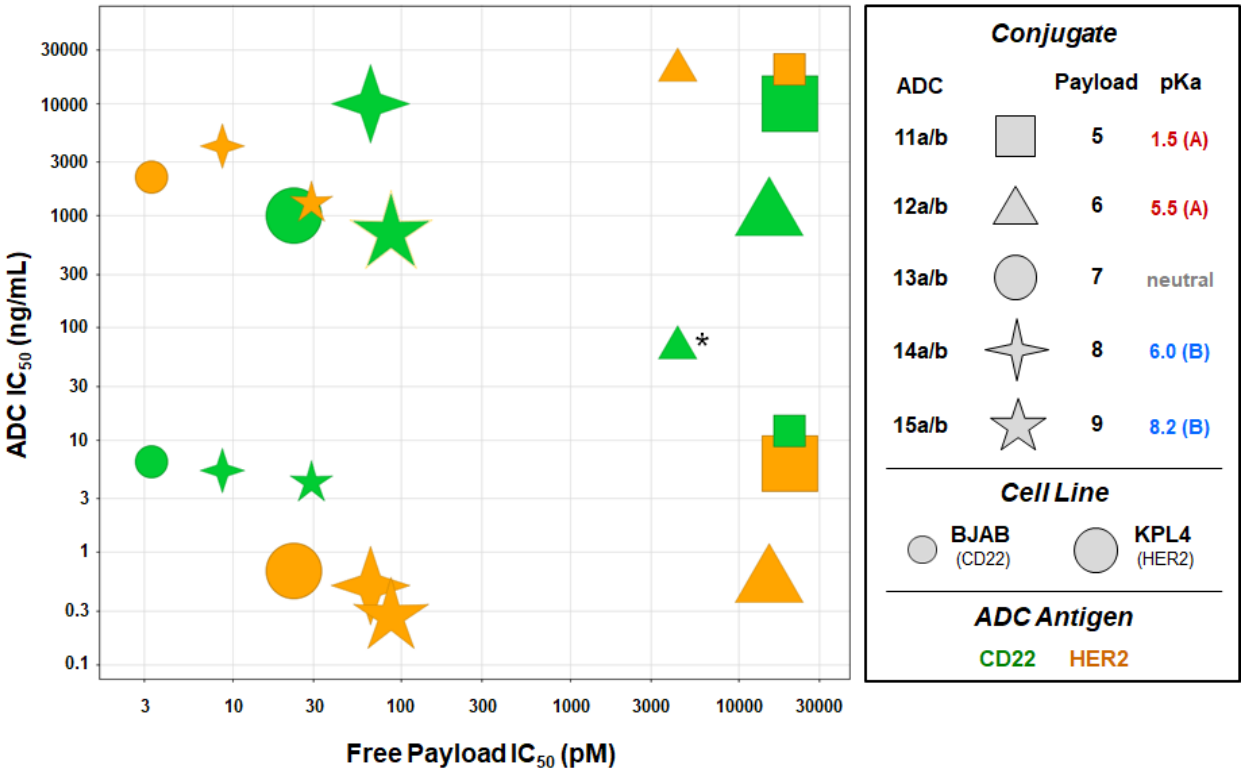

[a]Antiproliferation data are taken from Tables 1 and 2. The targeted antigen expressed by each cell line (CD22 or HER2) is listed below each name. pKa values refer to the R-group appended to each PBD-dimer payload and were calculated using the MoKa software package (version 2.6.6); **red** = acidic, **blue** = basic (conjugate acid). *Control ADC (**16a**) IC_{50} was weaker than typically observed; see Table 2 for additional details.

Strong *in vitro* antiproliferation potencies were also noted for the CD22-targeting conjugates whose PBD-dimer payloads contained added basic moieties. Both ADCs **14a** and **15a** were equipotent with conjugate **13a** for which the payload was the control molecule bearing the neutral methyl R-group (Table 2, Figures 5 and 7). As with conjugate **11a** above, the *in vitro* activity of **15a** was unexpected since the corresponding unconjugated payload associated with the latter ADC exhibited a low PAMPA Pe value at lysosomal pH (Table 1). Like conjugate **11a**, the potent activity of **15a** suggested efficient transition of the released payload from the lysosome to the cellular cytosol and/or nucleus following antibody-mediated delivery by mechanisms that are not fully understood at this time (see above for some possibilities).

Importantly, potent antigen-dependent antiproliferation activities were also observed when the HER2-targeting conjugates **11b**-**15b** were tested against the KPL4 cell line (Table 2, Figure 5). The majority of the ADCs whose payloads contained ionizable groups were equipotent in the KPL4 assessments to the conjugate for which the payload lacked any added ionizable functionality (compare **12b**, **14b**, and **15b**, with **13b**; Table 2, Figure 5). The one possible exception to this trend was conjugate **11b** which exhibited an approximately 10-fold weaker KPL4 IC_{50} value relative to **13b** (Table 2, Figure 5). This result may reflect reduced lysosome-cytosol transition efficiency in the KPL4 cells for the sulfonic acid-containing PBD-dimer payload (**5**) corresponding to **11b** relative to what was observed in the BJAB line. However, the outcome may also be related to the reduced DNA alkylation activity displayed by payload **5** compared to the PBD-dimer associated with conjugate **13b** (compound **7**, Table 1). The described data mirrored results observed previously with maytansine-containing trastuzumab-MCC-DM1 (T-DM1) which generates a cell-impermeable catabolite but is nevertheless highly potent against the KPL4 cell line.[27c,29] Importantly, the KPL4 outcomes also

confirmed that the potent *in vitro* antiproliferation activities displayed by conjugates bearing the new PBD-dimer payloads were associated with cancers in addition to those of B-cell origin. Reassuringly, none of the tested conjugates were particularly active when tested against the Jurkat cell line which did not express either the CD22 or HER2 antigen to a significant degree (Table 2, Figure 5).[25,30]

We were curious to understand how the *in vitro* biological activities observed for the ADCs described above would translate into *in vivo* anti-tumor efficacy studies. As shown in Figure 8A, single intravenous administration of CD22-targeting conjugate **13a** (0.3 mg/kg) to mice bearing WSU-DLCL2 xenografts afforded strong and durable anti-tumor efficacy over an extended observation time period. Alternatively, administration of a matched dose of ADC **12a** resulted in considerably weaker *in vivo* activity against the same WSU-DLCL2 model. These outcomes contrasted with the *in vitro* studies described in Table 2 above in which the two conjugates exhibited highly similar WSU-DLCL2 antiproliferation potencies (when normalized relative to control conjugate activity). One possibility for the differing *in vitro* and *in vivo* anti-cancer results is a greater dependency on bystander effects for efficacy in the xenograft studies relative to the cell-culture environment. Based on the PAMPA (pH 7.4) and antiproliferation characterizations depicted in Table 1, the PBD-dimer released from **12a** (compound **6**) was not expected to permeate from cell to cell as effectively as the corresponding payload delivered by **13a** (compound **7**). Such intercellular transition differences may be magnified in the environment of the WSU-DLCL2 tumors relative to cell-culture assessments since a greater proportion of the xenografted tumor cells are likely not exposed to direct contact by the administered ADCs. Encouragingly, the *in vivo* WSU-DLCL2 efficacy of conjugate **12a** could be increased by administering a higher dose to the test animals (compare 1.0 mg/kg efficacy

outcomes with the 0.3 mg/kg results, Figure 8A). Consistent with the involvement of bystander effects in WSU-DLCL2 efficacy outcomes, the activity of conjugate **11a** (bearing the least cell-permeable PBD-dimer payload **5**; c.f., Table 1) was attenuated relative to that observed for ADC **12a** when 1.0 mg/kg doses of the two conjugates were compared (Figure 8A). Importantly, all the conjugates tested in these initial *in vivo* assessments exhibited minimal effects on mouse body weights during the course of the studies (Figure 8B).

Figure 8. *In vivo* activity of conjugates **11a**, **12a**, and **13a** in the WSU-DLCL2 xenograft model.

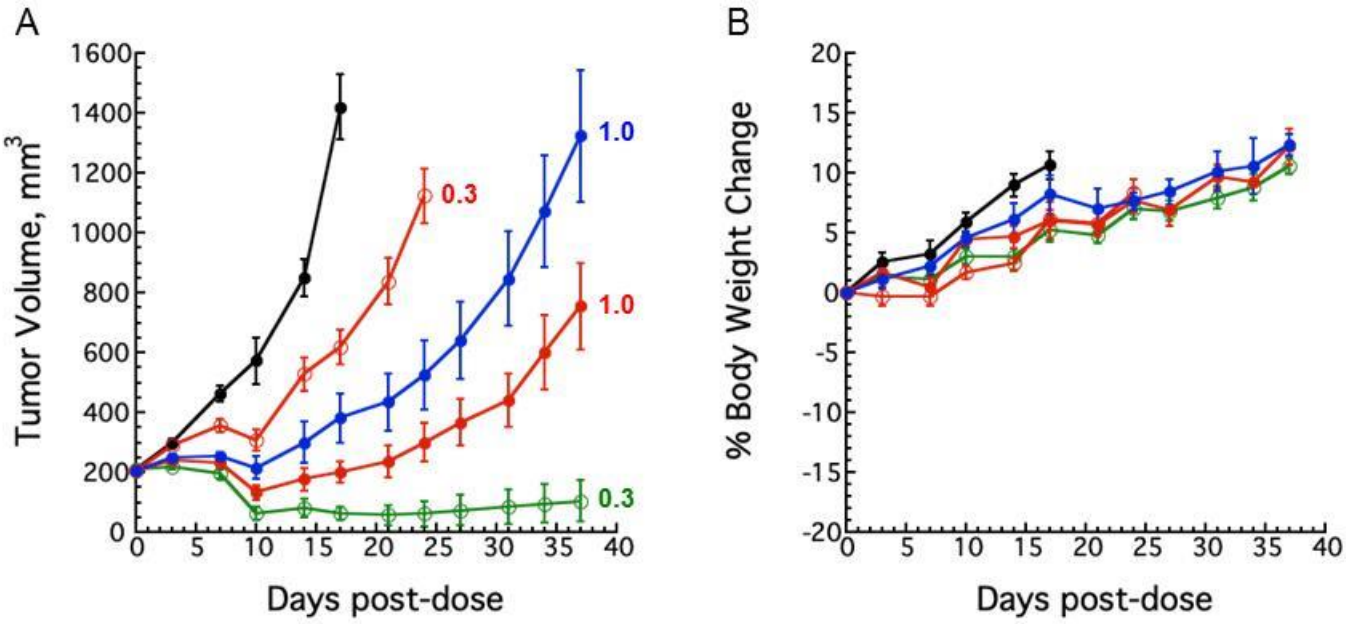

A. Efficacy (tumor growth inhibition). B. Impact on mouse body weights. **Blue traces**: **11a**, **red traces**: **12a**, **green traces**: **13a**, **black traces**: vehicle control. Numbers next to traces indicate doses of each conjugate (in mg/kg) that were administered once IV at the day 0 time point. Group mean tumor volumes or body weight changes (+/- SEM) are plotted over the duration of study (n=8/group). See Experimental section for additional details.

Figure 9. *In vivo* activity of conjugates **11a**, **11b**, **13a**, and **13b** in the WSU-DLCL2 xenograft model.

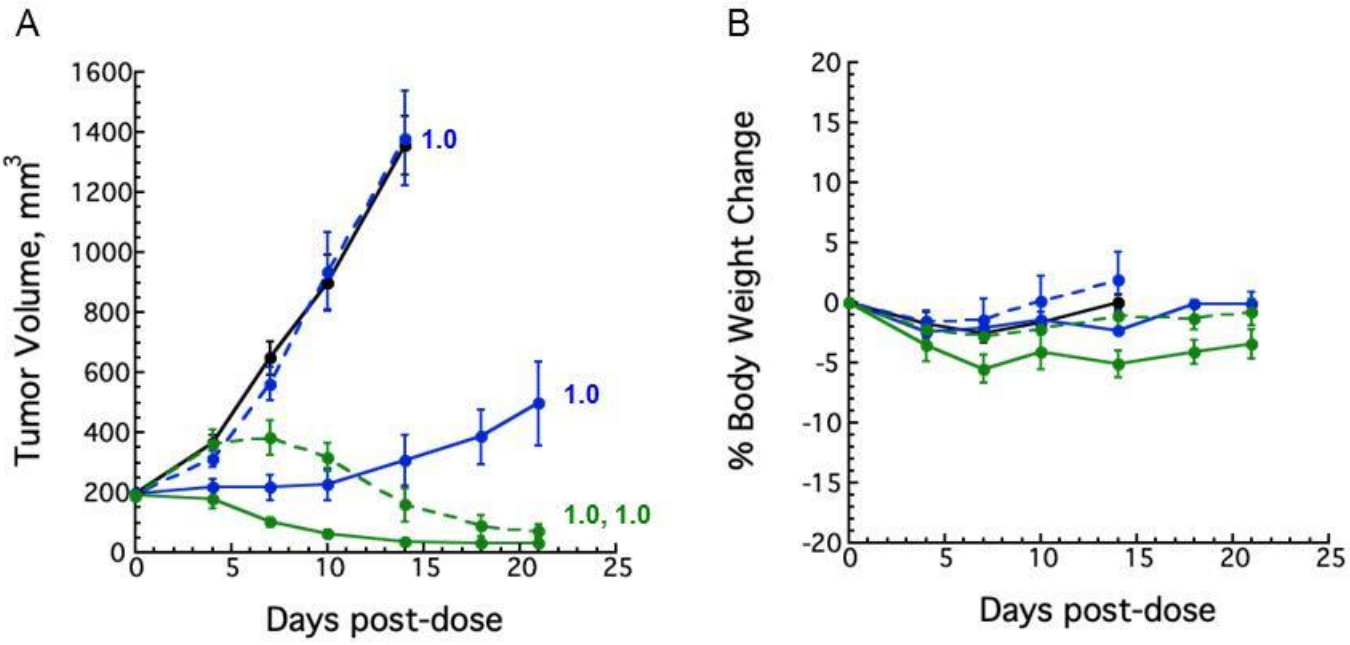

A. Efficacy (tumor growth inhibition). B. Impact on mouse body weights. **Blue traces** (solid line): **11a**, **Blue traces** (dotted line): **11b**, **green traces** (solid line): **13a**, **green traces** (dotted line): **13b**; **black traces**: vehicle control. Numbers next to traces indicate doses of each conjugate (in mg/kg) that were administered once IV at the day 0 time point. Group mean tumor volumes (+/- SEM) are plotted over the duration of study (n=5/group). See Experimental section for additional details.

Intrigued by the above observations, we further probed the impact of the payload modifications on *in vivo* activity by conducting a second xenograft study using the WSU-DLCL2 model. Figure 9A depicts the efficacy outcomes that were observed when conjugates **11a** and **13a** were tested at the 1.0 mg/kg dose level in this new experiment. As was observed in our initial *in vivo* assessment of the two conjugates, the anti-tumor efficacy displayed by **11a** (bearing the less cell-permeable payload) was attenuated relative to the activity exhibited by **13a**. We also compared the performance of HER2-targeting control conjugates **11b** and **13b** in this

experiment (both administered at 1.0 mg/kg) and were surprised to observe the highly disparate outcomes depicted in Figure 9A for the two ADCs. Specifically, strong *in vivo* efficacy was noted for **13b** that was similar to that observed for ADC **13a** at the later time points of the study. In contrast, the HER2-targeting **11b** displayed no *in vivo* efficacy, and the poor performance of this conjugate was easily distinguished from that of the related and much-more-active CD22-targeting ADC (**11a**). Stability assessments performed with conjugates **11a** and **13a** confirmed minimal deconjugation of the attached linker-drugs seven days after their administration to mice (Figure S2). In addition, no obvious biotransformations of the PBD-dimer payloads were observed in these studies. Similar excellent *in vivo* stability properties are expected to be associated with all conjugates described in this work. Collectively, these data suggested that the permeability differences associated with the PBD-dimer payloads delivered by conjugates **11a** and **13a** (compounds **5** and **7**, respectively; Table 1) may have influenced the antigen-independent activities of the corresponding HER2 conjugates (**11b** and **13b**) in this WSU-DLCL2 *in vivo* experiment. However, we did not compare the *in vivo* activities of **11b** and **13b** at lower doses (a 0.3 mg/kg dose of the related CD22 conjugate **13a** is sufficient to regress the WSU-DLCL2 tumor model; Figure 8A), and we cannot rule out that the outcomes observed with **13b** are simply a result of over-dosing the conjugate. As was the case with our initial assessments in this tumor model with conjugates **11a**, **12a**, and **13a**, it is possible that bystander effects contributed to the observed non-specific outcomes shown in Figure 9 and such phenomena were minimized by the poor cell permeability associated with the PBD-dimer payload delivered by conjugates **11a** and **11b**. Interestingly, the activity displayed by conjugates **11b** and **13b** in the *in vivo* experiment paralleled the *in vitro* antiproliferation outcomes observed for the ADCs (and the corresponding CD22-targeting conjugates) in non-specific activity

assessments employing Jurkat cells which did not express either the HER2 or CD22 antigens (i.e., **13a**/**13b** were more potent than **11a**/**11b**, Table 2, Figure 5). As was also observed in our initial *in vivo* assessments, all the conjugates tested in these subsequent WSU-DLCL2 experiments did not significantly impact mouse body weights over the duration of the studies (although minor body weight loss was noted for conjugate **13a** when administered at the 1.0 mg/kg dose level, Figure 9B).

Figure 10. *In vivo* activity of conjugates **13a**, **14a**, and **15a** in the WSU-DLCL2 xenograft model.

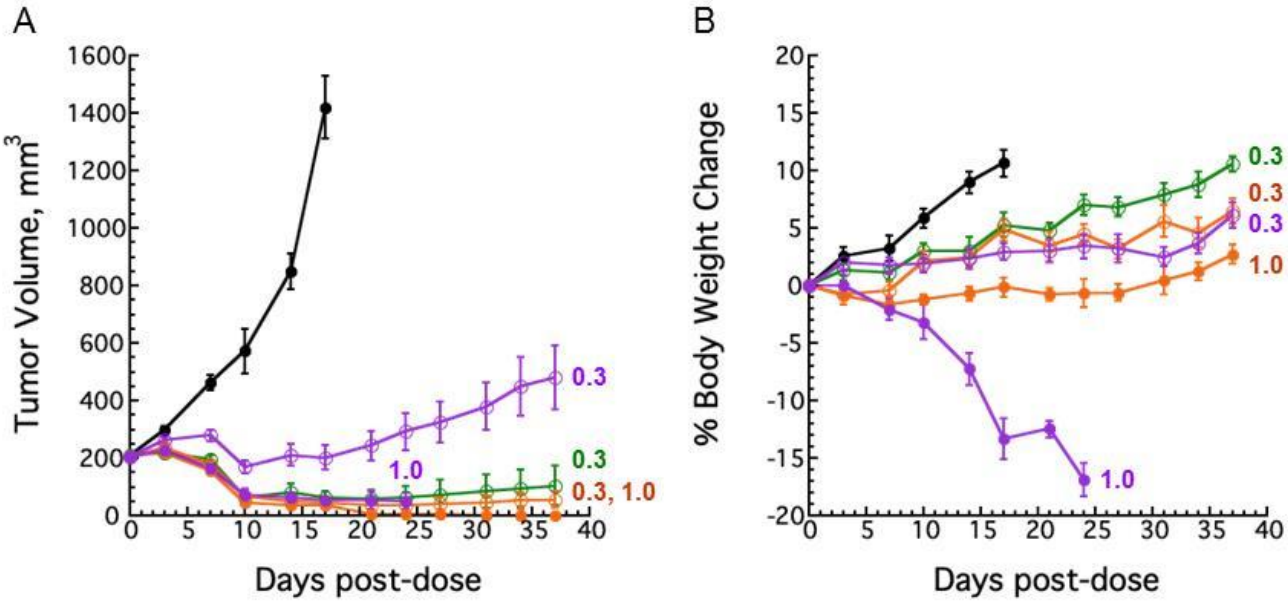

A. Efficacy (tumor growth inhibition). B. Impact on mouse body weights. **Green traces**: **13a**, **orange traces**: **14a**, **purple traces**: **15a**, **black traces**: vehicle control. Numbers next to traces indicate doses of each conjugate (in mg/kg) that were administered once IV at the day 0 time point. Group mean tumor volumes (+/- SEM) are plotted over the duration of study (n=5/group). See Experimental section for additional details.

To complete our *in vivo* assessments of the conjugates bearing the new PBD-dimer payloads, we profiled ADCs **13a**, **14a**, and **15a** in the WSU-DLCL2 xenograft model. All of the tested conjugates exhibited strong efficacy in these assessments following single IV administrations at relatively low doses (Figure 10A). Consistent with the efficacy outcomes associated with ADCs whose PBD-dimer payloads contained acidic functional groups, conjugate **15a** (bearing the least-permeable and strongly basic PBD-dimer) displayed somewhat attenuated *in vivo* antitumor activity relative to **13a** and **14a** at the 0.3 mg/kg dose (Figure 10A; c.f., Table 1). More strikingly, conjugate **15a** also had a much more deleterious impact on mouse body weights as compared to **13a** and **14a** when the ADCs were administered at the 1.0 mg/kg dose level (Figures 9B and 10B). Collectively, these data indicated that introduction of a strongly basic moiety into the PBD-dimer payload structure simultaneously worsened the *in vivo* efficacy and mouse tolerability outcomes of the corresponding ADCs as compared to conjugates bearing unmodified (neutral) PBD-dimer molecules. These outcomes may be related to the propensity of strongly basic small-molecules to indiscriminately bind to acidic tissue constituents (e.g., membrane phospholipids) and/or accumulate in acidic cellular compartments such as the lysosome.[31] Similarly, basic radioactive labels were observed to be widely distributed to the tissues of xenografted mice following administration of the corresponding radiolabeled antibodies.[32] Additional studies involving other PBD-dimer scaffolds, alternate *in vivo* efficacy models, and more-complete toxicology assessments are required to fully assess the generality of these observations. However, the current data suggest that improvements in the preclinical performance of PBD-dimer-containing ADCs can be realized by not including strongly basic moieties in the associated payloads.

Scheme 1. Synthesis of unconjugated PBD-dimers **5**-**9**.[a]

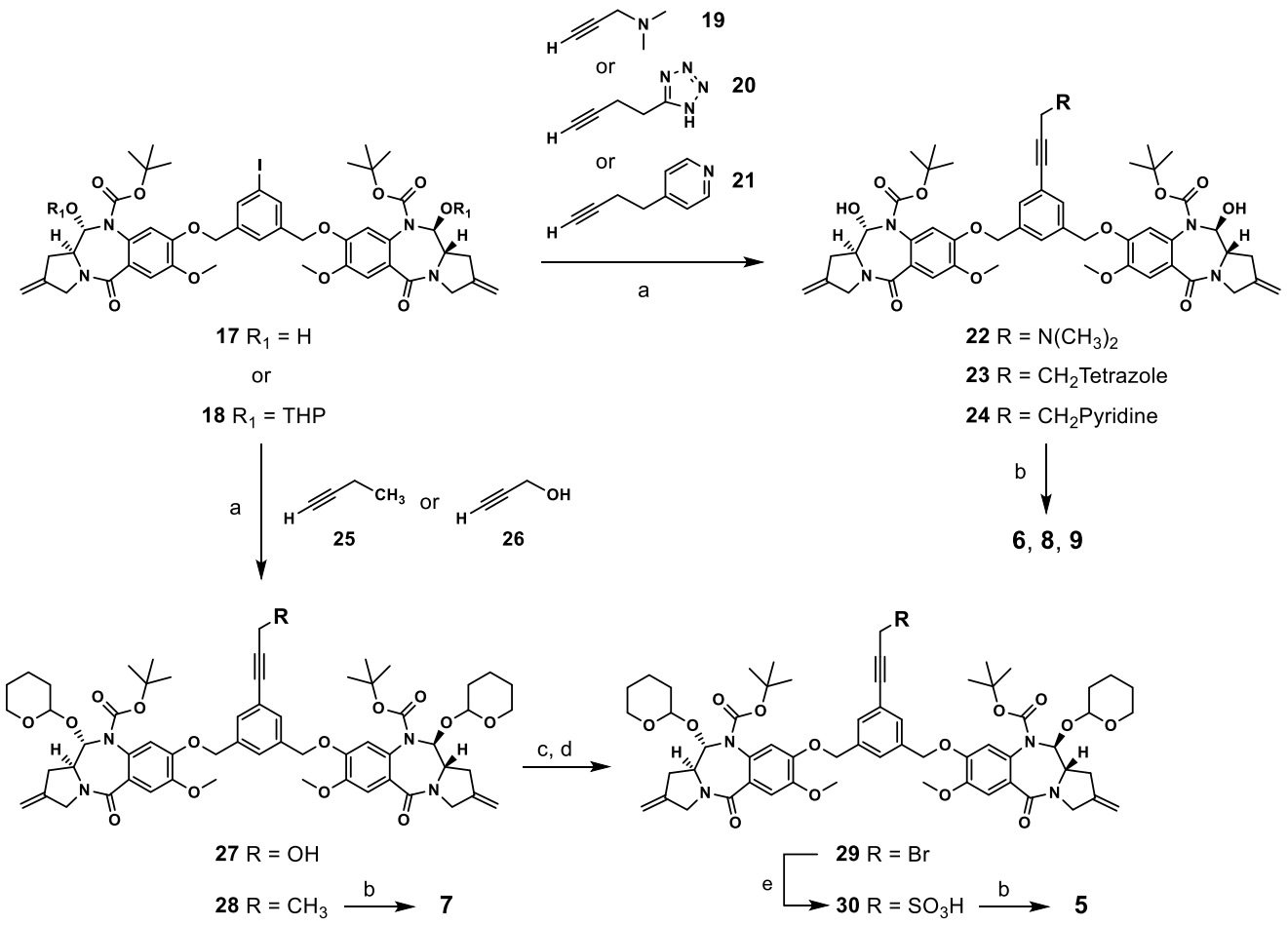

[a]Reagents and conditions: (a) alkyne, Et_2NH, $Pd(Ph_3P)_4$, CuI, DMF, 100 °C, 10-20 min, 40-67%; (b) TFA, 0-15 °C, 1 h, 15-80%; (c) Et_3N, MsCl, DCM, 15 °C, 0.5 h; (d) LiBr, THF, 10 °C, 16 h, 94%; (e) Na_2SO_3, 3:1 MeOH:H_2O, 60 °C, 6 h, 31%. THP = 2-tetrahydropyran.

The unconjugated PBD-dimers described in this work were prepared by the methods depicted in Scheme 1. For the synthesis of compounds **6**, **8**, and **9**, iodo-containing intermediate **17** (prepared as depicted in Scheme 4) was coupled to various alkynes (**19**-**21**) using well-precedented protocols.[33] Subsequent removal of the Boc protecting groups present in the

coupling products (**22-24**) afforded the desired PBD-dimers. The 1-dimethylamino-2-propyne (**19**) required for the synthesis of **22** was obtained from commercial sources while the preparations of alkynes **20** [5-(but-3-yn-1-yl)-1H-tetrazole] and **21** [4-(but-3-yn-1-yl)pyridine] are described in Scheme 5 below. Alternatively, the known THP-containing intermediate **18**[18] was similarly coupled to commercially available propargyl alcohol (**25**) or 1-butyne (**26**) to respectively give products **27** and **28**. The latter entity was deprotected under acidic conditions to afford PBD-dimer **7**. The former compound was transformed into sulfonic acid **29** (via propargyl bromide **28**), and the THP moieties present in **29** were subsequently removed to give PBD-dimer **5**.

Scheme 2. Preparation of antibody-drug conjugates **11a-15a** and **11b-15b**.[a]

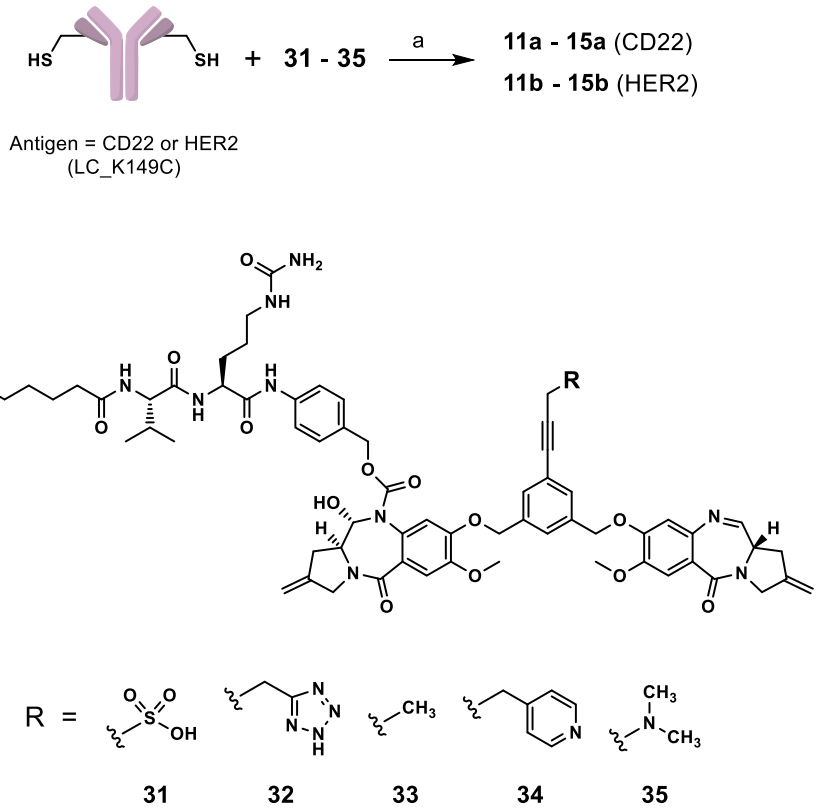

[a]Reagents and conditions: (a) DMF, Tris pH 6.5 to 7.5, 25 °C, 3-24 h.

The ADCs described in this work were prepared by conjugating anti-CD22 10F4v3 LC-K149C or anti-HER2 7C2 LC-K149C mAbs to linker-drugs **31**-**35** via the engineered LC-K149C cysteine residues according to previously published protocols (Scheme 2).[34] ADCs produced using the conjugation reaction conditions and purification schemes typically afforded protein yields of 25 to 95%. All of the conjugates were characterized in regards to aggregation (SEC HPLC), drug to antibody ratio (LCMS), and amount of unconjugated (free) drug present in the final conjugates (LCMS). Detailed characterization data for each conjugate are provided in Table S4 (Supporting Information).

The linker-drugs required for the preparation of the ADCs described in this work were synthesized by the methods depicted in Scheme 3. The nitro groups present in intermediate **36** (prepared as shown in Scheme 4) were reduced to afford the corresponding bis-aniline compound (**37**), and this entity was mono-protected in moderate yield by exposure to one equivalent of di-*tert*-butyl dicarbonate to give **38**. Transformation of the unprotected aniline contained in **38** to the corresponding isocyanate (or possibly the carbamic chloride) followed by condensation with commercially available Boc-Val-Cit-PAB-OH afforded carbamate **39** in reasonable yield. The silyl protecting groups present in **39** were removed under acidic conditions to generate diol **40**, and this intermediate was oxidized with IBX[35] to give compound **41**. As detailed in Scheme 1 for the unconjugated PBD-dimers, coupling of **41** with alkynes **19**, **20**, **21**, and **25** (Scheme 1) was accomplished using Sonogoshira protocols[33] to afford compounds **43b**-**43e** in good-to-moderate yields. The sulfonic acid-containing linker-drug **43a** was prepared by directly coupling prop-2-yne-1-sulfonic acid **42** (prepared as described in Scheme 5 below) to **41** in contrast to the related multi-step synthesis employed in Scheme 1 to generate the corresponding unconjugated PBD-dimer **5**. Removal of the Boc protecting groups present in

compounds **43a**-**43e** followed by coupling of the deprotected intermediates (not shown) to commercially available 6-maleimidocaproic acid *N*-hydroxysuccinate ester afforded the desired linker-drugs **31**-**35** in low-to-moderate yield following purification by preparative HPLC methods.

Scheme 3. Preparation of linker-drugs **31**-**35**.[a]

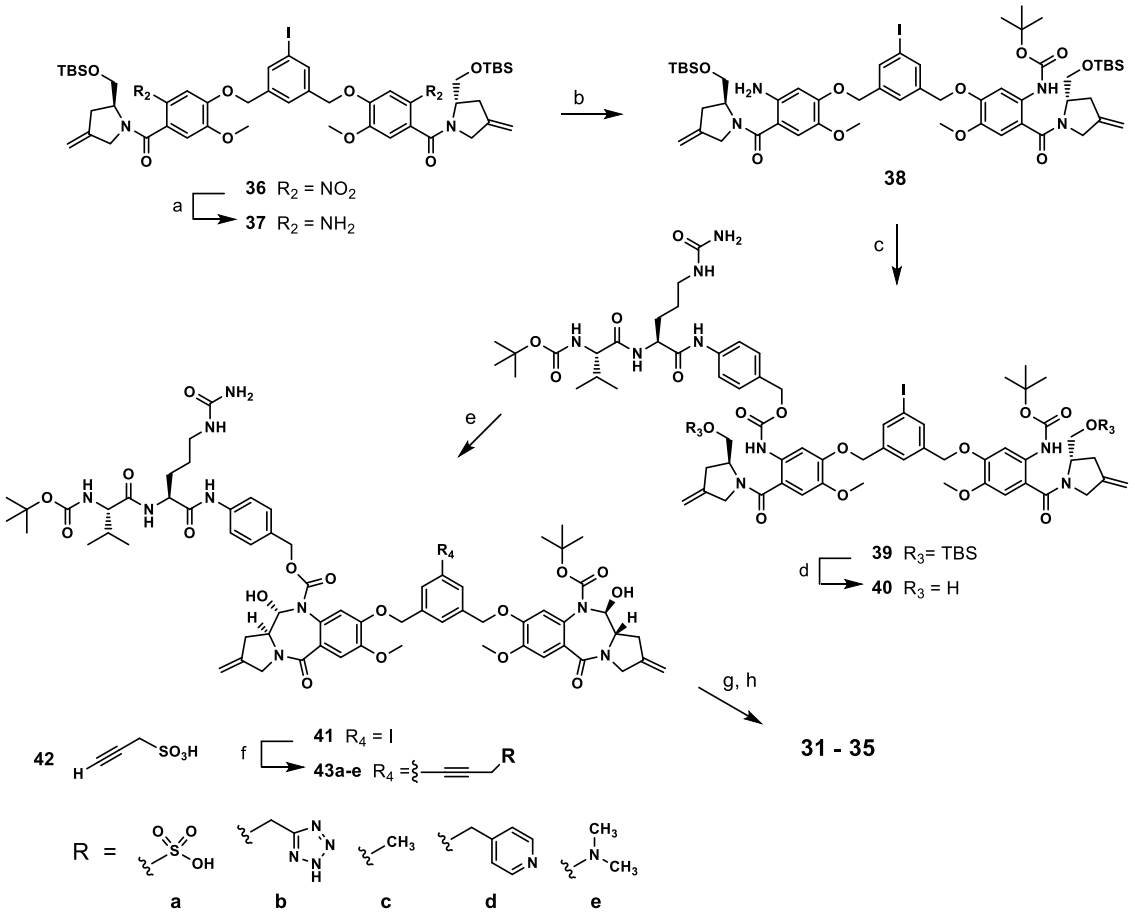

[a]Reagents and conditions: (a) Fe, NH_4Cl, 2:1 EtOH:H_2O, 80 °C, 2 h, 100%; (b) Boc_2O, THF, 75 °C, 3 h, 36%; (c) Et_3N, triphosgene, 4A sieves, DCM, 25 °C, 1 h, then Boc-Val-Cit-PAB-OH, DMF, 25 °C, 16 h, 81%; (d) HOAc, 3:1 THF:H_2O, 25 °C, 16 h, 79%; (e) IBX, DMSO, 38 °C, 16 h, 43%; (f) alkyne, Et_2NH, $Pd(Ph_3P)_4$, CuI, DMF, 25 °C, 12-48 h, 25-61%; (g) TFA, 0 °C, 1 h; (h) MC-OSu, (*i*-Pr)$_2$NEt, DMF, 25 °C, 10-72 h, 15-32%. TBS = $Si(CH_3)_2tBu$.

The syntheses of intermediates **17** and **36** required for the preparation of unconjugated PBD-dimers and related linker-drugs described above are illustrated in Scheme 4. Commercially available di-ester **44** was reduced to afford diol **45** which was subsequently transformed into di-bromide **46** in moderate overall yield on >100 g scale.[36] Coupling of **46** with commercially available 4-hydroxy-3-methoxybenzaldehyde (vanillin) provided intermediate **47**, and this entity was oxidized via the combination of $NaClO_2$, $NaH_2PO_4 \bullet 2H_2O$, and H_2O_2, to give di-acid **48** in good yield. Nitration of **48** proceeded smoothly to afford the di-nitro-di-acid **49** in moderate yield. This entity was converted to the corresponding di-acid-chloride (not shown) which was then coupled with trifluoroacetic acid salt **50** (prepared from the corresponding Boc-protected pyrrolidine;[37] not shown) to give intermeiate **51**. The acetate protecting groups present in the crude material thus obtained were removed via mild basic hydrolysis, and the resulting diol (**52**) was subsequently converted to the bis-*tert*-butyl-dimethylsilyl ether (intermediate **36**). Reduction of the nitro groups present in **36** followed by protection of the resulting anilines as the corresponding Boc-derivatives afforded intermediate **53** in good overall yield. Removal of the silyl protecting groups present in **53** followed by oxidation of the resulting diol (not shown) with the Dess-Martin periodinane[35] provided intermediate **17** in moderate yield after purification by preparative thin layer chromatography.

Scheme 4. Preparation of intermediates **17** and **36**.[a]

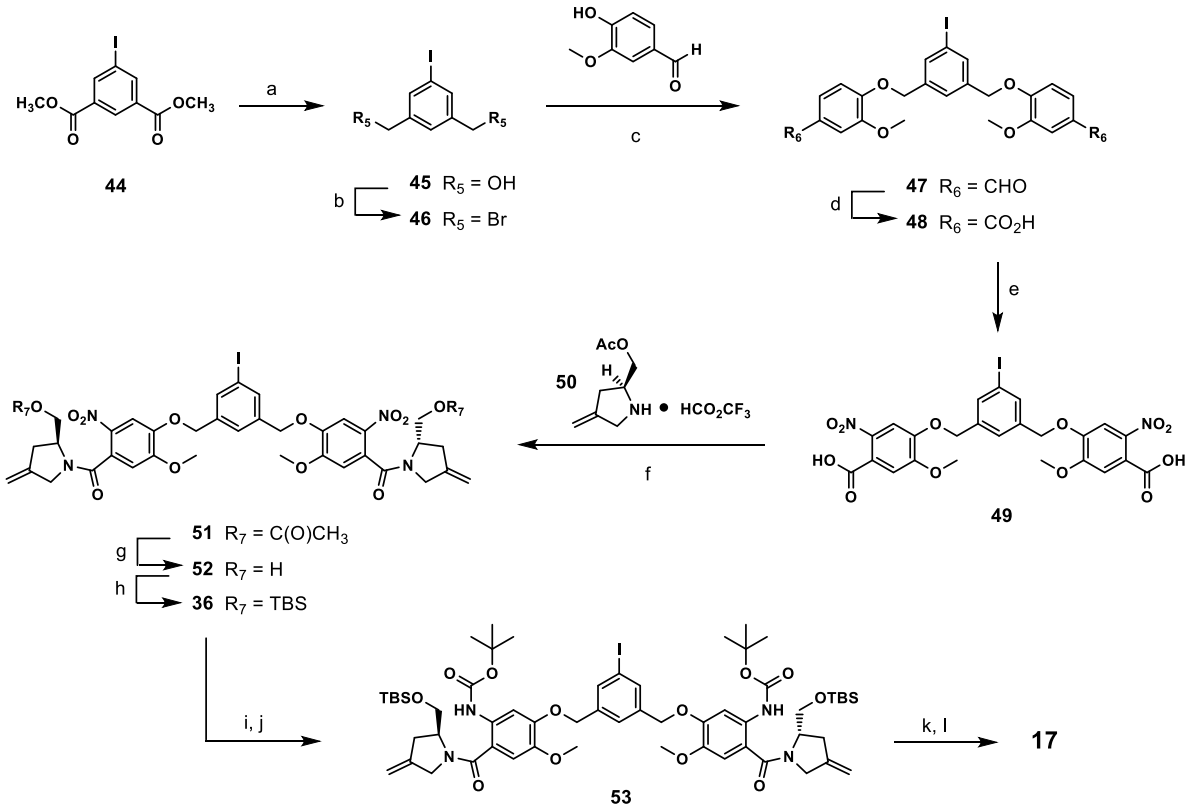

[a]Reagents and conditions: (a) $NaBH_4$, $CaCl_2$, EtOH, 0-25 °C, 2 h, 72%; (b) CBr_4, PPh_3, DCM, 0-25 °C, 12 h, 35%; (c) *n*-Bu_4NI, K_2CO_3, DMF, 60 °C, 6 h, 63%; (d) $NaClO_2$, NaH_2PO_4•$2H_2O$, H_2O_2, THF, 25-45 °C, 4 h, 93%; (e) HNO_3, 25 °C, 16 h, 58%; (f) oxalyl chloride, DCM, 25 °C, 4 h, then **50**, Et_3N, -40 to 0 °C, crude; (g) LiOH•$2H_2O$, 1:1 THF:H_2O, 25 °C, 3 h, 50% over 2 steps; (h) TBSCl, imidazole, DMF, 0-25 °C, 3 h, 67%; (i) Fe, NH_4Cl, 2:1 EtOH:H_2O, 90 °C, 2 h, 78%; (j) Boc_2O, THF, 90 °C, 6 h, 99%; (k) HOAc, 2:1 THF:H_2O, 18 °C, 48 h, 90%; (l) DMP, DCM, 14 °C, 16 h, 53%. TBS = $Si(CH_3)_2tBu$.

Scheme 5. Preparation of alkynes **20**, **21**, and **42**.[a]

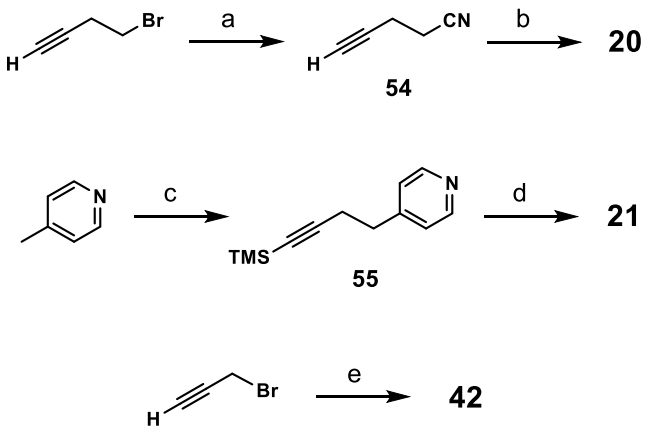

[a]Reagents and conditions: (a) NaI, DMSO, 0-20 °C, 2 h, then NaCN, 80 °C, 2 h, 54%; (b) $Et_3N{\bullet}HCl$, NaN_3, toluene, 25-115 °C, 10 h, 52%; (c) *n*-BuLi, $(i\text{-Pr})_2NH$, THF, -78 to 50 °C, 45 min, then (3-bromoprop-1-yn-1-yl)trimethylsilane, 20 °C, 3 h, 23%; (d) $n\text{-Bu}_4NF$, THF, 20 °C, 20 min, 99%; (e) Na_2SO_3, 1:1 MeOH:H_2O, 80 °C, 8 h, 98%.

CONCLUSION

This work describes the systematic variation of PBD-dimer physicochemical properties in an effort to better understand how such modifications impact the *in vitro* and *in vivo* performance of antibody-drug conjugates derived from the new compounds. The presented results complement a recent disclosure by others which explored PBD-dimer lipophilicity modulation as a means to improve conjugation efficiencies.[16] As demonstrated by the conducted experiments and resulting data, alterations which significantly ameliorated the antiproliferation activities of the unconjugated PBD-dimer molecules (presumably due to poor cell membrane permeability properties) had relatively little impact on the *in vitro* cell potencies of the corresponding ADCs. These results paralleled those reported previously for other ADC payload classes such as

auristatins and maytansinoids. A greater influence of these changes was noted *in vivo* with conjugates bearing low-permeable PBD-dimers exhibiting reduced xenograft efficacy relative to ADCs derived from payloads which exhibited more favorable membrane permeability characteristics. The former conjugates also displayed the largest activity differences when compared to the corresponding non-targeting control ADCs in the *in vivo* assessments. In spite of their attenuated potencies, conjugates derived from PBD-dimer payload **5** (containing the sulfonic acid moiety) were nevertheless active in both *in vitro* and *in vivo* assessments. Such conjugates, along with related new entities derived from **5**, thus enable the biological exploration of PBD-dimer-containing ADCs which release free payloads that are devoid of bystander effects. Importantly, introduction of a strongly basic amine moiety into the PBD-dimer payload structure significantly worsened mouse tolerability outcomes of the related ADCs relative to conjugates derived from less-basic PBD-dimer molecules. It is expected that this collective information will enable the design of new PBD-dimer-containing ADCs with improved therapeutic potential relative to existing entities.

EXPERIMENTAL SECTION

General Chemistry Methods. Unless otherwise indicated, all reagents and solvents were purchased from commercial sources and were used without further purification. Moisture or oxygen sensitive reactions were conducted under an atmosphere of argon or nitrogen gas. Unless otherwise stated, ^{1}H NMR spectra were recorded at 300 or 400 MHz using Varian or Bruker instruments operating at the indicated frequencies. Chemical shifts are expressed in ppm (δ) relative to an internal standard; tetramethylsilane (ppm = 0.00). The following abbreviations are used: br = broad signal, s = singlet, d = doublet, dd = doublet of doublets, t = triplet, q = quartet, p = pentet, m = multiplet. Purification by silica gel chromatography was carried out using Biotage systems with pre-packed cartridges. Chemical purities were ≥95% for all final compounds as assessed by LCMS analysis at UV 220 nm.

Molecular Modeling. Based on the solution structure of PBD-monomer covalently bound to a standard B-DNA helix (PBD entry 2KTT),[38] models of PBD-dimer variants (**5-9**) bound in the DNA minor grove were created as previously described.[18] For example, in the model for **7**, two covalent bonds (bond length 1.47-1.49 Å) between the C11/C11′ atom of two PBD-monomers and the exocyclic N2 atom of two deoxyguanines, which are separated by four base pairs on opposite DNA strands, serve to anchor the PBD-dimer snugly inside the minor groove.

PAMPA Testing. PAMPA permeability for DNA alkylators was determined using previously published method (Pion, Inc.). The compound concentration was 50 µM dissolved in 100 mM phosphate buffer before filtering. The receiver pH was 7.4 and donor pH was either 4 or 7.4. The incubation was performed at 37 °C for 4 h. The amount of compound permeated through the membrane was quantified by relative UV absorbance at 250-500 nm and the permeability Pe was calculated using the formula below.

$$P_e = \frac{-\ln[1 - C_A / C_{equilibrium}]}{S * (1/V_D + 1/V_A) * t}$$

Pe = permeability (cm/s)

V_D = donor volume (0.3 mL)

V_A = donor volume (0.2 mL)

$C_{equilibrium} = [(C_D * V_D) – (C_A * V_A)] / V_D – V_A$

S = membrane area (0.3 cm^2)

t = incubation time (sec)

DNA Alkylation Assessments. Two complementary single-strand DNA oligonucleotides (Oligo 1: 5'-TATAGAAATCTATA-3' and Oligo 2: 3'-ATATCTTTAGATAT-5') were synthesized at Genentech as designed previously.[19] The compounds **1** and **5-10** were incubated at 100 µM with double stranded DNA Oligos 1 and 2 (100 µM) for 1 hour in Bis-Tris buffer pH 7.1 (10 mM) at 37 °C. The samples were analyzed by LC-MS/UV (210-450 nm) on a Sciex TripleTOF 5600 mass spectrometer. The LC conditions were as follows: Hypersil Gold C18 column (100 x 2.1 mm, 1.9 µm, Thermo Scientific), flow rate of 0.4 mL/min and mobile phases A (50 mM hexafluoro-isopropanol and 15 mM diethylamine) and B (50% A and 50% of 1:1 methanol:acetonitrile) with a gradient of 5% B 0-0.5 min, 5- 25% B 0.5-25 min, 25-95% B 25-40 min, and 95% B 40-42 min. The measured percent remaining value determined for each compound was an average of the starting DNA oligos remaining in incubations (n = 2) compared to those in the control incubations of compound **10** (variability was <10% between

measurements). The products were characterized by LC/MS in a negative ESI ion mode. Under these conditions, all small molecules were eluted in the column wash after the gradient.

Antiproliferation Experiments (unconjugated compounds). Cells were seeded in 384-well plates and treated with unconjugated compounds 24 h later. After 4 days of continuous drug incubation, the cell viabilities were determined using CellTiter Glo II® reagent (Promega; Madison, WI). The luminescent intensities were measured on PerkinElmer Envision reader. The relative cell viabilities were calculated by normalizing to non-drug treatment controls and were graphed using KleidaGraph software package. The IC_{50} values were determined as the concentrations required to obtain 50% of the maximum cell killing.

Antiproliferation Experiments (conjugates). On day 0, suspension cell lines, BJAB (CD22-positive) and WSU-DLCL2 (CD22-positive) cells and Jurkat (CD22 and HER2-negative) cells, were seeded at 4000 cells per well in 40 µL RPMI-1640 culture media supplemented with 10% fetal bovine serum, 2 mM glutamine, 50 µM cystine, and 0.015 g/L L-methionine in 384-well flat clear bottom white polystyrene tissue culture-treated microplates (Corning, NY). Antibody-drug conjugates, 2 mg/mL in 20 mM Histidine Acetate, 240 mM Sucrose, 0.02% PS20 pH 5.5 buffer, were transferred to cells seeded in 384-well plates using ECHO acoustic liquid handling technology (Labcyte Inc, Sunnyvale, CA) to create a 10-point dose-response curve in triplicate starting from 20 µg/mL with 1:3x serial dilution. Cells were cultured in a humidified incubator set at 37 °C and maintaining an atmosphere of 5% CO_2. On day 4, cells were equilibrated to room temperature, then 40 µL/well CellTiter Glo II® reagent (Promega; Madison, WI) was added, and plates were shaken for 10 min then incubated for 30 min at RT in the dark. Luminescence was read using an EnVision 2101 Multilabel Reader (PerkinElmer, Waltham,

MA). Normalized luminescence intensity data were analyzed using GraphPad Prism 6, and IC_{50} values were calculated using a four parameter sigmoidal fit.

KPL4 (HER2-positive) cells were plated in black-walled 96-well plates and allowed to adhere overnight at 37 °C in a humidified atmosphere of 5% CO_2. The medium was then removed and replaced by fresh culture medium containing different concentrations of antibody-drug conjugates. After 5 days, CellTiter Glo® reagent (Promega Corp.) was added to the wells for 10 min at room temperature and the luminescent signal was measured using EnVision Multilabel Plate Reader (PerkinElmer).

In Vivo Efficacy Studies. All animal studies were carried out in compliance with National Institutes of Health guidelines for the care and use of laboratory animals and were approved by the Institutional Animal Care and Use Committee at Genentech, Inc.

The efficacy of the anti-CD22-drug conjugates was evaluated in a mouse xenograft model of CD22-expressing WSU-DLCL2 human non-Hodgkin lymphoma. The WSU-DLCL2 cell line was obtained from DSMZ (German Collection of Microorganisms and Cell Cultures; Braunschweig, Germany). To set up the xenograft model, tumor cells (20 million cells in 0.2 mL Hank's Balanced Salt Solution; Hyclone) were inoculated subcutaneously into the flanks of female C.B-17 SCID mice (Charles Rivers Laboratories). When tumors reached the desired volume (~200 mm^3), animals were divided into groups of 5-8 mice with similar mean tumor size and received a single intravenous injection of antibody-drug conjugates through the tail vein (referred to as Day 0). The treatment information was not blinded during tumor measurement. Tumors were measured in two dimensions (length and width) using calipers, and the tumor volume was calculated using the formula: tumor size (mm^3) = 0.5 x (length x width x width). Changes in mouse body weights were reported as a percentage relative to the starting weight.

Tumor sizes and mouse weights were recorded over the course of the study. Mice whose tumor volumes exceeded 2000 mm^3 or whose body weight losses were 20% of their starting weight were promptly euthanized per IACUC guidelines. Results were plotted as mean (± SEM) tumor volume or body weight change of each group over time.

Blood samples were collected via retro-orbital bleeds from animals and were used to derive plasma for *in vivo* ADC stability assessments. All blood samples were collected into tubes containing lithium heparin and were allowed to sit on wet ice until centrifugation (within 15 minutes of collection). Samples were centrifuged at 10,000 rpm for 5 minutes at 4 ºC. Plasma was then collected, placed on dry ice, and stored in a freezer set at -70 ºC until analysis.

Compound Syntheses. The preparation of unconjugated PBD-dimer **9** is provided below as a representative example of the syntheses of compounds **6**, **8**, and **9**. Characterization data for compounds **6** and **8** are provided following the information associated with **9**. The preparations of the required non-commercial alkynes (**20** and **21**; Scheme 5) are described at the end of the compound synthesis section.

*di-tert-Butyl 8,8'-(((5-(3-(dimethylamino)prop-1-yn-1-yl)-1,3-phenylene)bis(methylene))-bis(oxy))(11S,11aS,11'S,11a'S)-bis(11-hydroxy-7-methoxy-2-methylene-5-oxo-2,3,11,11a-tetrahydro-1H-benzo[e]pyrrolo[1,2-a][1,4]diazepine-10(5H)-carboxylate) (**22**).* $Pd(PPh_3)_4$ (25.9 mg, 0.02 mmol) was added to a mixture of compound **17** (110 mg, 0.11 mmol), 1-dimethylamino-2-propyne (**19**, 47 mg, 0.56 mmol), Et_2NH (164 mg, 2.24 mmol), CuI (4.3 mg, 0.02 mmol) and 4Å MS (30 mg) in anhydrous DMF (3 mL). The reaction mixture was heated via microwave irradiation at 100 °C under N_2 for 10 min then was cooled to 25 °C. The mixture was filtered, and the filtrate was concentrated *in vacuo* to remove the solvent. The residue was then diluted with EtOAc (100 mL), and the resulting solution was washed with brine (30 mL x

4), dried over Na_2SO_4, filtered, and concentrated. The crude material thus obtained was purified by prep-HPLC (acetonitrile 35-65/10 mM NH_4HCO_3 in water) to give compound **22** (70 mg, 67%) as a white solid. LCMS (5-95, AB, 1.5 min): RT = 0.80 min, $[M+H]^+$ 936.7.

*(11aS,11a'S)-8,8'-(((5-(3-(Dimethylamino)prop-1-yn-1-yl)-1,3-phenylene)bis-(methylene))bis(oxy))bis(7-methoxy-2-methylene-1,2,3,11a-tetrahydro-5H-benzo[e]pyrrolo[1,2-a][1,4]diazepin-5-one) (**9**).* A solution of compound **22** (70 mg, 0.07 mmol) in TFA (3 mL) was stirred at 15 °C for 1 h. The solution was added dropwise to saturated aqueous $NaHCO_3$ solution (200 mL) at 0 °C, and the resulting mixture was extracted with DCM (40 mL x 3). The combined DCM layers were dried over Na_2SO_4, filtered, and were concentrated. Purification of the residue by prep-TLC (10% MeOH in DCM, R_f = 0.5) afforded compound **9** (43 mg, 80%) as a white solid. LCMS (5-95, AB, 1.5 min): RT = 0.73 min, $[M+H]^+$ 700.3. ^1H NMR (400 MHz, $CDCl_3$) δ 7.65 (d, *J* = 4.0 Hz, 2H), 7.52 (s, 2H), 7.47 - 7.44 (m, 3H), 6.80 (s, 2H), 5.19 - 5.10 (m, 8H), 4.28 (s, 4H), 3.96 (s, 6H), 3.88 - 3.86 (m, 2H), 3.49 (s, 2H), 3.14 - 3.08 (m, 2H), 2.95 - 2.91 (m, 2H), 2.38 (s, 6H).

*(11aS,11a'S)-8,8'-(((5-(4-(1H-Tetrazol-5-yl)but-1-yn-1-yl)-1,3-phenylene)bis-(methylene))bis(oxy))bis(7-methoxy-2-methylene-1,2,3,11a-tetrahydro-5H-benzo[e]pyrrolo[1,2-a][1,4]diazepin-5-one) (**6**).* LCMS (5-95, AB, 1.5min): RT = 0.783 min, [M+H] + 739.3.

*(11aS,11a'S)-8,8'-(((5-(4-(Pyridin-4-yl)but-1-yn-1-yl)-1,3-phenylene)bis(methylene))-bis(oxy))bis(7-methoxy-2-methylene-1,2,3,11a-tetrahydro-5H-benzo[e]pyrrolo[1,2-a][1,4]diazepin-5-one) (**8**).* LCMS (5-95, AB, 1.5 min): RT = 0.755 min, $[M+H]^+$ 748.4. ^1H NMR (400 MHz, $CDCl_3$) δ 8.53 (d, *J* = 5.6 Hz, 2H), 7.66 (d, *J* = 4.8 Hz, 2H), 7.53 (s, 2H), 7.42 (s, 1H), 7.38 (s, 2H), 7.21 (d, *J* = 5.6 Hz, 2), 6.80 (s, 2H), 5.19 - 5.09 (m, 8H), 4.28 (s, 4H), 3.96 (s, 6H), 3.89 - 3.86 (m, 2H), 3.10 - 3.08 (m, 2H), 2.95 - 2.91 (m, 4H), 2.74 - 2.70 (m, 2H).

The preparation of unconjugated PBD-dimer **5** is provided below to illustrate the synthesis of this compound as well as compound **7**. Characterization data for compound **7** follow the information associated with **5**.

*di-tert-Butyl 8,8'-(((5-(3-hydroxyprop-1-yn-1-yl)-1,3-phenylene)bis(methylene))bis(oxy))-(11S,11aS,11'S,11a'S)-bis(7-methoxy-2-methylene-5-oxo-11-((tetrahydro-2H-pyran-2-yl)oxy)-2,3,11,11a-tetrahydro-1H-benzo[e]pyrrolo[1,2-a][1,4]diazepine-10(5H)-carboxylate) (**27**).* $Pd(PPh_3)_4$ (40 mg, 0.03 mmol) was added to a mixture of compound **18**[18] (200 mg, 0.17 mmol), propargyl alcohol (**26**, 256 mg, 3.08 mmol), Et_2NH (254 mg, 3.48 mmol), CuI (6.6 mg, 0.03 mmol) and 4Å MS (50 mg) in anhydrous DMF (3 mL). The reaction mixture was heated via microwave irradiation at 100 °C under N_2 for 15 min then was cooled to 25 °C. The mixture was filtered, and the filtrate was concentrated *in vacuo*. The residue was diluted with EtOAc (50 mL), and the resulting solution was washed with H_2O (30 mL x 4), dried over Na_2SO_4, filtered, and concentrated *in vacuo*. The residue was purified by prep-TLC (5 % MeOH in DCM, R_f = 0.5) to give compound **27** (120 mg, 60%) as a white solid. LCMS (5-95, AB, 1.5 min): RT = 1.02 min, $[M+Na]^+$ 1099.8.

*di-tert-Butyl 8,8'-(((5-(3-bromoprop-1-yn-1-yl)-1,3-phenylene)bis(methylene))bis(oxy))-(11S,11aS,11'S,11a'S)-bis(7-methoxy-2-methylene-5-oxo-11-((tetrahydro-2H-pyran-2-yl)oxy)-2,3,11,11a-tetrahydro-1H-benzo[e]pyrrolo[1,2-a][1,4]diazepine-10(5H)-carboxylate) (**29**).* To a 15 °C solution of compound **27** (120 mg, 0.11 mmol) in anhydrous DCM (10 mL) was added Et_3N (338 mg, 3.34 mmol) followed by dropwise addition of methanesulfonyl chloride (280 mg, 2.44 mmol). The reaction solution was stirred at 15 °C for 0.5 h then was diluted with DCM (50 mL). The resulting mixture was washed with H_2O (20 mL x 3), dried over Na_2SO_4, filtered, and concentrated *in vacuo* to give the crude mesylate (128 mg, 94%). To a solution of this crude

material in anhydrous THF (10 mL) at 10 °C was added LiBr (48 mg, 0.55 mmol). The reaction solution was stirred at that temperature for 16 h whereupon it was diluted with DCM (50 mL). The resulting mixture was washed with H_2O (20 mL x 3), dried over Na_2SO_4, filtered, and concentrated *in vacuo* to give crude compound **29** (126 mg, 94%). LCMS (5-95, AB, 1.5 min): RT = 1.11 min, $[M+Na]^+$ 1161.2. This material was used in the next step without further purification.

*3-(3,5-bis((((11S,11aS)-10-(tert-Butoxycarbonyl)-7-methoxy-2-methylene-5-oxo-11-((tetrahydro-2H-pyran-2-yl)oxy)-2,3,5,10,11,11a-hexahydro-1H-benzo[e]pyrrolo[1,2-a][1,4]diazepin-8-yl)oxy)methyl)phenyl)prop-2-yne-1-sulfonic acid (**30**).* To a mixture of compound **29** (126 mg, 0.11 mmol) in MeOH (15 mL) / water (5 mL) at 25 °C was added Na_2SO_3 (139 mg, 1.11 mmol). The reaction mixture was stirred at 60 °C for 6 h. After cooling to 25 °C, the mixture was concentrated *in vacuo* to remove MeOH. The remaining aqueous slurry was then extracted with DCM (50 mL x 4). The combined DCM layers were dried over Na_2SO_4, filtered, and were concentrated. The residue was purified by prep-TLC (10% MeOH in DCM, R_f = 0.3) followed by prep-HPLC (acetonitrile 40-70/10 mM NH_4HCO_3 in water) to afford compound **30** (40 mg, 31%) as a white solid. LCMS (5-95, AB, 1.5 min): RT = 0.98 min, $[M-2Boc-2THP-2H_2O+H]^+$ 737.1.

*3-(3,5-bis((((S)-7-Methoxy-2-methylene-5-oxo-2,3,5,11a-tetrahydro-1H-benzo[e]pyrrolo-[1,2-a][1,4]diazepin-8-yl)oxy)methyl)phenyl)prop-2-yne-1-sulfonic acid (**5**).* A solution of compound **30** (25 mg, 0.02 mmol) in TFA (2 mL) / water (0.10 mL) was stirred at 15 °C for 1 h. The solution was concentrated *in vacuo* to remove the solvent, and the residue was first pH-adjusted to 9.0 by addition of saturated aqueous $NaHCO_3$ solution (2 mL), then was further diluted with H_2O (8.0 mL). The resulting solution was purified by prep-HPLC (acetonitrile 20-

50 % in water) to afford compound **5** (sodium salt, 5 mg, 27%) as a white solid. LCMS (5-95, AB, 1.5 min): RT = 0.75 min, $[M+H]^+$ 737.3.

(11aS,11a'S)-8,8'-(((5-(But-1-yn-1-yl)-1,3-phenylene)bis(methylene))bis(oxy))bis(7-methoxy-2-methylene-1,2,3,11a-tetrahydro-5H-benzo[e]pyrrolo[1,2-a][1,4]diazepin-5-one) (7). LCMS (5-95, AB, 1.5 min): RT = 0.88 min, $[M+H]^+$ 671.4.

The preparation of linker-drug **35** is provided below as a representative example of the syntheses of compounds **31**-**35**. As part of these preparations, intermediate **41** was derivatized with the appropriate alkyne to afford compounds **43a-43e**. The required alkynes were commercially available [1-dimethylamino-2-propyne (**19**) and but-1-yne (**25**); Scheme 1] or were synthesized as described at the end of the chemical synthesis section (**20**, **21**, and **42**; Scheme 5). Characterization data for compounds **31-34** are provided following the information associated with **35**.

((((5-Iodo-1,3-phenylene)bis(methylene))bis(oxy))bis(2-amino-5-methoxy-4,1-phenylene))bis(((S)-2-(((tert-butyldimethylsilyl)oxy)methyl)-4-methylenepyrrolidin-1-yl)methanone) (37). To a mixture of compound **36** (preparation described below; 5.00 g, 4.66 mmol) in EtOH (50 mL) / water (25 mL) was added iron (2.60 g, 47 mmol), followed by NH_4Cl (4.98 g, 93 mmol). The reaction mixture was stirred at 80 °C for 2 h then was concentrated to remove most of the EtOH. The residue was filtered, washed with EtOAc (60 mL), and the filtrate was diluted with H_2O (40 mL). The resulting mixture was extracted with EtOAc (60 mL x 3), and the combined organic layers were dried over Na_2SO_4, filtered, and were concentrated to afford compound **37** (4.70 g, 100%) as a pale yellow solid. LCMS (5-95, AB, 1.5 min): RT = 1.16 min, $[M+H]^+$ 1013.4.

*tert-Butyl (5-((3-((5-amino-4-((S)-2-(((tert-butyldimethylsilyl)oxy)methyl)-4-methylenepyrrolidine-1-carbonyl)-2-methoxyphenoxy)methyl)-5-iodobenzyl)oxy)-2-((S)-2-(((tert-butyldimethylsilyl)oxy)methyl)-4-methylenepyrrolidine-1-carbonyl)-4-methoxyphenyl)carbamate (**38**).* To a 25 °C solution of compound **37** (4.70 g, 4.64 mmol) in anhydrous THF (100 mL) was added Boc_2O (1.01 g, 4.64 mmol). The reaction solution was stirred at 75 °C for 3 h then was cooled to 25 °C and was concentrated under vacuum. The residue was purified by chromatography on silica gel (10-60 % EtOAc in petroleum ether) to afford compound **38** (2.00 g, 36%) as a pale yellow solid. LCMS (5-95, AB, 1.5 min): RT = 1.15 min, $[M+H]^+$ 1113.3. A portion of starting material **37** (2.3 g) was also recovered by subsequently eluting the silica gel column with a more polar solvent mixture (0-40 % MeOH in DCM).

*tert-Butyl (5-((3-((5-((((4-((S)-2-((S)-2-((tert-butoxycarbonyl)amino)-3-methylbutanamido)-5-ureidopentanamido)benzyl)oxy)carbonyl)amino)-4-((S)-2-(((tert-butyldimethylsilyl)oxy)methyl)-4-methylenepyrrolidine-1-carbonyl)-2-methoxyphenoxy)methyl)-5-iodobenzyl)oxy)-2-((S)-2-(((tert-butyldimethylsilyl)oxy)methyl)-4-methylenepyrrolidine-1-carbonyl)-4-methoxyphenyl)carbamate (**39**).* A solution of compound **38** (400 mg, 0.36 mmol) and Et_3N (182 mg, 1.8 mmol) in anhydrous DCM (10 mL) was added dropwise to a 25 °C solution of triphosgene (106 mg, 0.36 mmol) and 4 Å MS (30 mg) in anhydrous DCM (20 mL). The reaction mixture was stirred at 25 °C for 1 h then was concentrated under vacuum. The crude product thus obtained was used directly in the next step without further purification. To the above crude product (409 mg, 0.36 mmol) in anhydrous DCM (8.0 mL) was added Et_3N (109 mg, 1.08 mmol) followed by a solution of commercially available *tert*-butyl ((*S*)-1-(((*S*)-1-((4-(hydroxymethyl)phenyl)amino)-1-oxo-5-ureidopentan-2-yl)amino)-3-methyl-1-oxobutan-2-yl)carbamate (Boc-Val-Cit-PAB-OH, 258 mg, 0.54 mmol) in anhydrous DMF (8.0 mL). After

the reaction mixture was stirred at 20 °C for 16 h, it was concentrated under reduced pressure. The residue was purified by chromatography on silica gel (0-15% MeOH in DCM) to give compound **39** (500 mg, 81%) as a white solid. LCMS (5-95, AB, 1.5 min): RT = 1.14 min, [(M-100)/2+H]$^+$ 759.7.

*tert-Butyl (5-((3-((5-(((((4-((S)-2-((S)-2-((tert-butoxycarbonyl)amino)-3-methylbutanamido)-5-ureidopentanamido)benzyl)oxy)carbonyl)amino)-4-((S)-2-(hydroxymethyl)-4-methylenepyrrolidine-1-carbonyl)-2-methoxyphenoxy)methyl)-5-iodobenzyl)oxy)-2-((S)-2-(hydroxymethyl)-4-methylenepyrrolidine-1-carbonyl)-4-methoxyphenyl)carbamate (**40**).* To a solution of compound **39** (500 mg, 0.31 mmol) in THF (3.0 mL) / water (1.5 mL) was added HOAc (4.5 mL, 0.31 mmol). The reaction solution was stirred at 25 °C for 16 h then was concentrated under vacuum. The residue was purified by chromatography on silica gel (0-15% MeOH in DCM) to afford compound **40** (390 mg, 79%) as a pale yellow solid. LCMS (5-95, AB, 1.5 min): RT = 0.94 min, [M+H]$^+$ 1390.7.

*4-((S)-2-((S)-2-((tert-Butoxycarbonyl)amino)-3-methylbutanamido)-5-ureidopentanamido)benzyl(11S,11aS)-8-((3-((((11S,11aS)-10-(tert-butoxycarbonyl)-11-*hydroxy-*7-methoxy-2-methylene-5-oxo-2,3,5,10,11,11a-hexahydro-1H-benzo[e]pyrrolo[1,2-a][1,4]diazepin-8-yl)oxy)methyl)-5-iodobenzyl)oxy)-11-hydroxy-7-methoxy-2-methylene-5-oxo-2,3,11,11a-tetrahydro-1H-benzo[e]pyrrolo[1,2-a][1,4]diazepine-10(5H)-carboxylate (**41**).* To a solution of compound **40** (100 mg, 0.07 mmol) in DMSO (8.0 mL) was added IBX (161 mg, 0.58 mmol) at 25 °C. The reaction was warmed to 38 °C and was stirred at that temperature for 16 h. The mixture was cooled to 25 °C and was poured into ice-water (15 mL). The resulting precipitate was collected by vacuum filtration and was purified by chromatography on silica gel (0-12 % MeOH in DCM) to give semi-pure product. This material was further purified by prep-

TLC (10% MeOH in DCM, R_f = 0.5) to give compound **41** (45 mg, 43%) as a white solid. LCMS (5-95, AB, 1.5 min): RT = 0.89 min, $[M+Na]^+$ 1408.5.

*4-((S)-2-((S)-2-((tert-Butoxycarbonyl)amino)-3-methylbutanamido)-5-ureidopentanamido)benzyl (11S,11aS)-8-((3-((((11S,11aS)-10-(tert-butoxycarbonyl)-11-hydroxy-7-methoxy-2-methylene-5-oxo-2,3,5,10,11,11a-hexahydro-1H-benzo[e]pyrrolo[1,2-a][1,4]diazepin-8-yl)oxy)methyl)-5-(3-(dimethylamino)prop-1-yn-1-yl)benzyl)oxy)-11-hydroxy-7-methoxy-2-methylene-5-oxo-2,3,11,11a-tetrahydro-1H-benzo[e]pyrrolo[1,2-a][1,4]diazepine-10(5H)-carboxylate (**43e**).* $Pd(Ph_3P)_4$ (20 mg, 0.02 mmol) was added to a mixture of compound **41** (120 mg, 0.090 mmol), Et_2NH (0.18 mL, 1.73 mmol), 1-dimethylamino-2-propyne (**19**, 36 mg, 0.43 mmol), and CuI (16 mg, 0.09 mmol) in anhydrous DMF (6.0 mL) at 25 °C. The reaction solution was stirred at 25 °C under N_2 for 16 h then was concentrated under vacuum. The residue was purified by prep-TLC (12% MeOH in DCM, R_f = 0.5) to afford compound **43e** (50 mg, 41%) as a brown solid. LCMS (5-95, AB, 1.5 min): RT = 0.81 min, $[(M+H]^+$ 1342.6.

*4-((S)-2-((S)-2-(6-(2,5-Dioxo-2,5-dihydro-1H-pyrrol-1-yl)hexanamido)-3-methylbutanamido)-5-ureidopentanamido)benzyl (11S,11aS)-8-((3-(3-(dimethylamino)prop-1-yn-1-yl)-5-((((S)-7-methoxy-2-methylene-5-oxo-2,3,5,11a-tetrahydro-1H-benzo[e]pyrrolo[1,2-a][1,4]diazepin-8-yl)oxy)methyl)benzyl)oxy)-11-hydroxy-7-methoxy-2-methylene-5-oxo-2,3,11,11a-tetrahydro-1H-benzo[e]pyrrolo[1,2-a][1,4]diazepine-10(5H)-carboxylate (**35**).* Part 1. A solution of compound **43e** (25 mg, 0.020 mmol) in TFA (1.5 mL, 0.02 mmol) was stirred at 0 °C for 1 h. The solution was added dropwise into saturated aqueous $NaHCO_3$ solution (40 mL) at 0 °C, and the resulting mixture was extracted with DCM/MeOH (10:1, 30 mL x 3). The combined organic layers were dried over Na_2SO_4, filtered, and were concentrated to give the crude deprotected product (structure not shown, 20 mg, 76%) as a brown solid. LCMS (5-95,

AB, 1.5 min): RT = 0.72 min, $[M/2+H]^+$ 562.5. Part 2. To a solution of the crude material prepared above (20 mg, 0.02 mmol) and commercially available 2,5-dioxopyrrolidin-1-yl 6-(2,5-dioxo-2,5-dihydro-1H-pyrrol-1-yl)hexanoate (MC-OSu, 27 mg, 0.09 mmol) in anhydrous DMF (4.0 mL) was added $(i\text{-Pr})_2$NEt (11 mg, 0.09 mmol) at 25 °C. The reaction solution was stirred at that temperature for 48 h then was concentrated under vacuum. The residue was purified by prep-TLC (12% MeOH in DCM, R_f = 0.4) to give semi-pure product. This material was combined with another batch of semi-pure product (prepared on the same scale from **43e** as described above) and the combined lots were again purified by prep-TLC (12% MeOH in DCM, R_f = 0.4) to afford compound **35** (12.5 mg) as a white solid. LCMS (5-95, AB, 1.5 min): RT = 0.78 min, $[M/2+H]^+$ 659.1.

*3-(3-((((11S,11aS)-10-(((4-((S)-2-((S)-2-(6-(2,5-Dioxo-2,5-dihydro-1H-pyrrol-1-yl)hexanamido)-3-methylbutanamido)-5-ureidopentanamido)benzyl)oxy)carbonyl)-11-hydroxy-7-methoxy-2-methylene-5-oxo-2,3,5,10,11,11a-hexahydro-1H-benzo[e]pyrrolo[1,2-a][1,4]diazepin-8-yl)oxy)methyl)-5-((((S)-7-methoxy-2-methylene-5-oxo-2,3,5,11a-tetrahydro-1H-benzo[e]pyrrolo[1,2-a][1,4]diazepin-8-yl)oxy)methyl)phenyl)prop-2-yne-1-sulfonic acid **(31)**.* LCMS (10-80, AB, 7.0 min): RT = 3.03 min, $[M/2+H]^+$ 677.8.

*4-((S)-2-((S)-2-(6-(2,5-Dioxo-2,5-dihydro-1H-pyrrol-1-yl)hexanamido)-3-methylbutanamido)-5-ureidopentanamido)benzyl (11S,11aS)-8-((3-(4-(1H-tetrazol-5-yl)but-1-yn-1-yl)-5-((((S)-7-methoxy-2-methylene-5-oxo-2,3,5,11a-tetrahydro-1H-benzo[e]pyrrolo[1,2-a][1,4]diazepin-8-yl)oxy)methyl)benzyl)oxy)-11-hydroxy-7-methoxy-2-methylene-5-oxo-2,3,11,11a-tetrahydro-1H-benzo[e]pyrrolo[1,2-a][1,4]diazepine-10(5H)-carboxylate **(32)**.* LCMS (5-95, AB, 1.5 min): RT = 0.70 min, $[M+Na]^+$ 1377.4.

*4-((S)-2-((S)-2-(6-(2,5-Dioxo-2,5-dihydro-1H-pyrrol-1-yl)hexanamido)-3-methylbutanamido)-5-ureidopentanamido)benzyl (11S,11aS)-8-((3-(but-1-yn-1-yl)-5-((((S)-7-methoxy-2-methylene-5-oxo-2,3,5,11a-tetrahydro-1H-benzo[e]pyrrolo[1,2-a][1,4]diazepin-8-yl)oxy)methyl)benzyl)oxy)-11-hydroxy-7-methoxy-2-methylene-5-oxo-2,3,11,11a-tetrahydro-1H-benzo[e]pyrrolo[1,2-a][1,4]diazepine-10(5H)-carboxylate (**33**).* LCMS (10-80, AB, 7.0 min): RT = 3.84 min, $[M/2+H]^+$ 644.6.

*4-((S)-2-((S)-2-(6-(2,5-Dioxo-2,5-dihydro-1H-pyrrol-1-yl)hexanamido)-3-methylbutanamido)-5-ureidopentanamido)benzyl (11S,11aS)-11-hydroxy-7-methoxy-8-((3-((((S)-7-methoxy-2-methylene-5-oxo-2,3,5,11a-tetrahydro-1H-benzo[e]pyrrolo[1,2-a][1,4]diazepin-8-yl)oxy)methyl)-5-(4-(pyridin-4-yl)but-1-yn-1-yl)benzyl)oxy)-2-methylene-5-oxo-2,3,11,11a-tetrahydro-1H-benzo[e]pyrrolo[1,2-a][1,4]diazepine-10(5H)-carboxylate (**34**).* LCMS (5-95, AB, 1.5 min): RT = 0.78 min, $[M/2+H]^+$ 682.9.

*(5-Iodo-1,3-phenylene)dimethanol (**45**).* To a 10-L 4-necked round-bottom flask was placed ethanol (2000 mL) at 0 °C followed by sequential addition of $NaBH_4$ (252 g, 6.66 mol) portionwise and commercially available 1,3-dimethyl-5-iodobenzene-1,3-dicarboxylate (**44**, 520 g, 1.62 mol) at the same temperature. To this mixture was added a solution of $CaCl_2$ (362 g) in ethanol (3000 mL) dropwise with stirring at 0 °C. The resulting solution was stirred at room temperature for 2 h then was quenched by the addition of 2000 mL of 0 °C water. The mixture was concentrated under vacuum, and the residue was diluted with water (1000 mL) and extracted with EtOAc (2000 mL x 3). The combined organic layers were dried over Na_2SO_4, filtered, and were concentrated under vacuum to afford compound **45** (310 g, 72%) as a white solid.

*1,3-bis(Bromomethyl)-5-iodobenzene (**46**).* To a 5000-mL 4-necked round-bottom flask purged and maintained with an inert atmosphere of nitrogen was placed a solution of compound

45 (310 g, 1.17 mol) in DCM (2000 mL) and CBr_4 (856 g) followed by the addition of a solution of triphenylphosphine (640 g, 2.45 mol) in DCM (1000 mL) dropwise with stirring at 0 °C. The resulting solution was stirred at room temperature overnight then was concentrated under vacuum. The residue was purified by chromatography on silica gel (5% EtOAc in petroleum ether) to afford compound **46** (160 g, 35%) as a white solid.

*4,4'-(((5-Iodo-1,3-phenylene)bis(methylene))bis(oxy))bis(3-methoxybenzaldehyde) (**47**).* To a 3000-mL 4-necked round-bottom flask was placed a solution of commercially available 4-hydroxy-3-methoxybenzaldehyde (vanillin, 80 g, 0.53 mol) in DMF (2000 mL), K_2CO_3 (74 g, 0.54 mol), TBAI (10 g, 27 mmol) and compound **46** (104 g, 0.27 mol). The resulting solution was stirred at 60 °C for 3 h, then additional portions of 4-hydroxy-3-methoxybenzaldehyde, K_2CO_3, and TBAI (same amounts as described previously) were sequentially added and stirring was continued at 60 °C for another 3 h. The reaction mixture was cooled to room temperature with a water bath and was quenched by the addition of water (1000 mL). The resulting mixture was extracted with EtOAc (1000 mL x 3), and the combined organic layers were dried over Na_2SO_4, filtered, and were concentrated under vacuum. Purification of the residue by chromatography on silica gel (16-50% EtOAc in DCM) afforded compound **47** (177 g, 63%) as a white solid.

*4,4'-(((5-Iodo-1,3-phenylene)bis(methylene))bis(oxy))bis(3-methoxybenzoic acid) (**48**).* To a 5000-mL 4-necked round-bottom flask was placed a solution of $NaClO_2$ (78 g,) in water (1400 mL) and $NaH_2PO_4 \cdot 2H_2O$ (52 g) followed by the addition of a solution of compound **47** (177 g, 333 mmol) in THF (2000 mL) dropwise with stirring at 25 °C. To this mixture was added H_2O_2 (30%, 887 mL) dropwise with stirring. The resulting solution was stirred at 45 °C for 4 h, then was cooled to at 25 °C and the pH was adjusted to 3 via the addition of aqueous HCl

(1 N). The resulting solution was extracted with EtOAc (1000 mL x 3), and the combined organic layers were dried over Na_2SO_4, filtered, and were concentrated under vacuum to afford compound **48** (175 g, 93%) as a white solid.

*4,4'-(((5-Iodo-1,3-phenylene)bis(methylene))bis(oxy))bis(5-methoxy-2-nitrobenzoic acid) (**49**).* To a 5000-mL 4-necked round-bottom flask was placed concentrated HNO_3 (2500 mL) followed by the addition of compound **48** (78 g, 137 mmol) in portions at 25 °C. The resulting solution was stirred at that temperature overnight then was quenched by the addition of 5 L of water/ice. The resulting solids were collected by vacuum filtration to afford compound **49** as a yellow solid. The reaction was repeated on the same scale to afford a second batch of **49** (combined yield = 104 g, 58%).

*(S)-(4-Methylenepyrrolidin-2-yl)methyl acetate trifluoroacetic acid salt (**50**).* To a 1000-mL 3-necked round-bottom flask purged and maintained with an inert atmosphere of nitrogen was placed a solution of *tert*-butyl (2*S*)-2-[(acetyloxy)methyl]-4-methylidenepyrrolidine-1-carboxylate[37] (64 g, 250 mmol,) in DCM (500 mL) followed by the addition of TFA (128 mL) dropwise with stirring at 0 °C. The resulting solution was then stirred at room temperature for 2 h after which it was concentrated under vacuum to afford 110 g of crude **50** as brown oil. This material was used without additional purification in the next step below.

*((2R,2'R)-(4,4'-(((5-Iodo-1,3-phenylene)bis(methylene))bis(oxy))bis(5-methoxy-2-nitrobenzoyl))bis(4-methylenepyrrolidine-1,2-diyl))bis(methylene) diacetate (**51**).* To a 3000-mL 4-necked round-bottom flask was placed compound **49** (77 g, 118 mmol) in DCM (1000 mL) followed by the addition of oxalyl chloride (70 g) dropwise with stirring at 25 °C. The resulting solution was stirred at that temperature for 4 h then was concentrated under vacuum. The residue was dissolved in DCM (1500 mL) to provide "solution A". To a separate 3000-mL 4-

necked round-bottom flask purged and maintained with an inert atmosphere of nitrogen was placed a solution of crude compound **50** (116 g, 430 mmol) in DCM (1000 mL) followed by the addition of Et_3N (168 g, 1.66 mol) dropwise with stirring at -40 °C. To this mixture was added "solution A" prepared above at -40 °C. The reaction was allowed to warm to 0 °C over 2 h, then was quenched by the addition of 0 °C water (1000 mL). The resulting mixture was extracted with DCM (2000 mL x 3), and the combined organic layers were dried over Na_2SO_4, filtered, and were concentrated under vacuum to afford crude compound **51** (130 g) as a yellow solid. This material was used in subsequent transformations without additional purification.

*((((5-Iodo-1,3-phenylene)bis(methylene))bis(oxy))bis(5-methoxy-2-nitro-4,1-phenylene))bis(((S)-2-(hydroxymethyl)-4-methylenepyrrolidin-1-yl)methanone) (**52**).* To a 2000-mL 4-necked round-bottom flask was placed a solution of compound **51** (130 g, 140 mmol) in THF/H_2O (500 mL / 500 mL) and LiOH•$2H_2O$ (23 g, 540 mmol). The resulting solution was stirred at 25 °C for 3 h then was extracted with EtOAc (500 mL x 3). The combined organic layers were dried over Na_2SO_4, filtered, and were concentrated under vacuum. The residue was purified by chromatography on silica gel (9% MeOH in DCM) to afford compound **52** (60 g, 50%) as a yellow solid.

*((((5-Iodo-1,3-phenylene)bis(methylene))bis(oxy))bis(5-methoxy-2-nitro-4,1-phenylene))bis(((S)-2-(((tert-butyldimethylsilyl)oxy)methyl)-4-methylenepyrrolidin-1-yl)methanone) (**36**).* To a 3000-mL 4-necked round-bottom flask purged and maintained with an inert atmosphere of nitrogen was placed a solution of compound **52** (60 g, 70 mmol) in DMF (1500 mL) followed by the addition of imidazole (57 g) in portions at 0 °C. To this mixture was added TBSCl (53.6 g) in portions at 0 °C. The resulting solution was stirred at 25 °C for 3 h then was quenched by the addition of water (5000 mL). The quenched reaction was extracted with

EtOAc (1000 mL x 3), and the combined organic layers were dried over Na_2SO_4, filtered, and were concentrated under vacuum. The residue was purified by chromatography on silica gel (33% EtOAc in petroleum ether) to afford compound **36** (51 g, 67%) as a light yellow solid. LCMS (60-95, AB, 6.6 min): RT = 3.07 min $[M+H]^+$, 1073.7. ^1H NMR (300 MHz, DMSO-d_6) δ 7.87 - 7.84 (m, 4H), 7.58 (s, 1H), 7.25 (s, 1H), 7.05 (s, 1H), 5.26 - 5.24 (m, 4H), 5.00 (s, 1H), 4.91 (s, 1 H), 4.39 - 4.21 (m, 2H), 3.94 - 3.93 (m, 6H), 3.86 - 3.83 (m, 4H), 3.79 - 3.47 (m, 3H), 3.39 - 3.32 (m, 1H), 2.72 - 2.60 (m, 2H), 2.50 (m, 1H), 0.88 (s, 12H), 0.73 (s, 6H), 0.084 (s, 8H), 0.07 (s, 4H), -0.16 (s, 2H), -0.21 (s, 2H).

*di-tert-Butyl ((((5-iodo-1,3-phenylene)bis(methylene))bis(oxy))bis(6-((S)-2-(((tert-butyldimethylsilyl)oxy)methyl)-4-methylenepyrrolidine-1-carbonyl)-4-methoxy-3,1-phenylene))dicarbamate (**53**).* To a mixture of compound **36** (3.00 g, 2.80 mmol) in EtOH (20 mL) / water (10 mL) was added iron (1.56 g, 28 mmol), followed by NH_4Cl (2.99 g, 55.9 mmol). The reaction mixture was stirred at 90 °C for 2 h. The mixture was filtered, and the filtrate was diluted with H_2O (50 mL) and extracted with EtOAc (80 mL x 3). The combined organic layers were dried over Na_2SO_4, filtered, and were concentrated *in vacuo* to give the bis-aniline-intermediate (structure not shown; 2.20 g, 78%) as a white solid. LCMS (5-95, AB, 1.5 min): RT = 1.20 min, $[M+H]^+$ 1013.5. Boc_2O (1.90 g, 8.69 mmol) was added to a solution of this crude material in anhydrous THF (50 mL), and the reaction solution was stirred at 90 °C for 6 h. The mixture was concentrated *in vacuo* to afford crude compound **53** (2.60 g, 99%) as a pale yellow solid. LCMS (5-95, AB, 1.5 min): RT = 1.43 min, $[M+H]^+$ 1214.8.

*di-tert-Butyl 8,8'-(((5-iodo-1,3-phenylene)bis(methylene))bis(oxy))(11S,11aS,11'S,11a'S)-bis(11-hydroxy-7-methoxy-2-methylene-5-oxo-2,3,11,11a-tetrahydro-1H-benzo[e]pyrrolo[1,2-a][1,4]diazepine-10(5H)-carboxylate) (**17**).* A solution of crude compound **53** (2.60 g, 2.14

mmol) in HOAc (15 mL) / THF (10 mL) / water (5 mL) was stirred at 18 °C for 48 h. The solution was diluted with EtOAc (120 mL), and was washed sequentially with H_2O (40 mL x 5) and saturated aqueous $NaHCO_3$ solution (30 mL x 2). The EtOAc layer was dried over Na_2SO_4, filtered, and was concentrated. The residue was purified by chromatography on silica gel (0 - 3.3% MeOH in DCM) to give the crude diol intermediate (1.90 g, 90%) as a yellow solid. LCMS (5-95, AB, 1.5 min): RT = 1.01 min, $[M+H]^+$ 985.3. To a solution of a portion of this crude material (400 mg, 0.41 mmol) in anhydrous DCM (40 mL) at 14 °C was added DMP (450 mg, 1.06 mmol). After the reaction mixture was stirred at that temperature for 16 h, it was diluted with H_2O (20 mL) followed by saturated aqueous Na_2SO_3 solution (20 mL) and saturated aqueous $NaHCO_3$ solution (20 mL). The mixture was extracted with EtOAc (60 mL x 3), and the combined organic layers were dried over Na_2SO_4, filtered, and were concentrated. The residue was purified by prep-TLC (7% MeOH in DCM, R_f = 0.7) to give compound **17** (220 mg, 53%) as a white solid. LCMS (5-95, AB, 1.5 min): RT = 0.93 min, $[M+Na]^+$ 1003.5.

*Pent-4-ynenitrile (**54**).* NaI (560 mg, 3.76 mmol) was added to a solution of 4-bromo-1-butyne (500 mg, 3.76 mmol) in DMSO (4.0 mL) at 0 °C. The mixture was warmed to 20 °C and was stirred at that temperature for 2 h. NaCN (368 mg, 7.52 mmol) was then added, and the mixture was warmed to 80 °C and maintained at that temperature for 2 h. After cooling to 20 °C, the reaction was stirred for an additional 18 h then was partitioned between EtOAc (20 mL) and water (10 mL). The organic layer was washed with water (5 mL x 4) and was dried over Na_2SO_4 and concentrated to give crude **54** (160 mg, 54%) as a brown oil. This material was used directly in next step.

*5-(But-3-yn-1-yl)-1H-tetrazole (**20**).* $Et_3N{\bullet}HCl$ (522 mg, 3.79 mmol) and NaN_3 (246 mg, 3.79 mmol) were added sequentially to a solution of crude compound **54** (100 mg, 1.26 mmol) in

toluene (5 mL) at 25 °C. The mixture was heated to 115 °C and was stirred at that temperature for 10 h. After cooling to 25 °C, the reaction mixture was partitioned between EtOAc (20 mL) and water (20 mL). The aqueous layer was then acidified with HOAc and HCl (2.0 M) to pH = 1.0 and was subsequently extracted with EtOAc (20 mL x 4). The combined organic layers were dried over Na_2SO_4 and were concentrated. The residue was purified by chromatography on silica gel (20% EtOAc in petroleum ether) to afford compound **20** (80 mg, 52%) as an orange solid. ^{1}H NMR (400 MHz, DMSO-d_6) δ 3.08 (t, J = 6.8 Hz, 2H), 2.84 (t, J = 2.8 Hz, 1H), 2.67-2.63 (m, 2H).

*4-(4-(Trimethylsilyl)but-3-yn-1-yl)pyridine (**55**).* A solution of *n*-BuLi in hexanes (0.94 mL, 2.36 mmol) was added dropwise to a solution of *N,N*-diisopropylamine (1.07 mL, 2.15 mmol) in anhydrous THF (10 mL) at -78 °C under N_2. The solution was stirred at 0 °C for 10 minutes. 4-Methylpyridine (200 mg, 2.15 mmol) in anhydrous THF (5 mL) was added dropwise, and the mixture was then heated to 50 °C for 45 min. The mixture was cooled to 20 °C, and (3-bromoprop-1-yn-1-yl)trimethylsilane (328 mg, 1.72 mmol) in anhydrous THF (5 mL) was added. The resulting mixture was stirred for another 3 h at 20 °C then was quenched with saturated NH_4Cl solution (20 mL). The quenched reaction was extracted with EtOAc (30 mL x 3), and the combined EtOAc layers were dried over Na_2SO_4, filtered, and were concentrated. The residue was purified by prep-TLC (33% EtOAc in petroleum ether, R_f = 0.4) to afford compound **55** (100 mg, 23%) as colorless oil. ^{1}H NMR (400 MHz, $CDCl_3$) δ 8.52 (d, J = 6.0 Hz, 2H), 7.17 (d, J = 5.6 Hz, 2H), 2.82 (t, J = 7.6 Hz, 2H), 2.53 (t, J = 7.6 Hz, 2H), 0.12 (s, 9H).

*4-(But-3-yn-1-yl)pyridine (**21**)*. TBAF (775 mg, 2.46 mmol) was added to a solution of compound **55** (100 mg, 0.490 mmol) in anhydrous THF (10 mL) at 20 °C. The reaction mixture was stirred at that temperature for 20 min then was diluted with DCM (60 mL). The resulting

solution was washed with H_2O (30 mL x 3), dried over Na_2SO_4, filtered, and was concentrated to afford crude 4-(but-3-yn-1-yl)pyridine **21** (64 mg, 99%) as a brown oil. This material was used in subsequent Sonogashira coupling reactions without additional purification.

*Sodium prop-2-yne-1-sulfonate (**42**).* A mixture of Na_2SO_3 (5.72 g, 45 mmol) and propargyl bromide (4.0 mL, 36 mmol) in MeOH (14 mL) and water (14 mL) was heated to 80 °C for 8 h. MeOH (200 mL) was added and the precipitate was filtered off. The filtrate was concentrated to about 10 mL then acetone (200 mL) was added, and the resulting precipitate was collected by vacuum filtration to give the desired product **42** (5.00 g, 98%) as a white solid. ^{1}H NMR (400 MHz, D_2O) δ 3.84 (t, J = 2.8 Hz, 2H), 2.70 (t, J = 2.8 Hz, 1H).

ASSOCIATED CONTENT

The Supporting Information is available free of charge on the ACS Publications website at DOI: XXX.

95% confidence intervals for Table 1 IC_{50} data, antiproliferation activity of compounds **5**-**9** against a panel of cancer cell lines, 95% confidence intervals for Table 2 IC_{50} data, CD22 expression in WSU-DLCL2 cells, *in vivo* stability for conjugates **11a** and **13a**, conjugate characterization data (PDF)

Molecular formula strings of Table 1 compounds (**5**-**10**) (CSV)

Molecular formula strings of new compounds in Schemes 1-5 (CSV)

AUTHOR INFORMATION

Corresponding author

Phone: 650-467-6854, Email: dragovich.peter@gene.com

ORCID

Peter S. Dragovich: 0000-0001-7372-2862

Katherine R. Kozak: 0000-0003-3751-7225

Thomas H. Pillow: 0000-0001-7300-1002

Notes

The authors declare no competing financial interest.

ACKNOWLEDGEMENTS

The authors would like to thank members of the Genentech and WuXi Biologics Conjugation Groups for the preparation and characterization of the antibody-drug conjugates described in this work.

ABBREVIATIONS USED

Boc_2O, di-*tert*-butyl dicarbonate; DAR, drug-antibody ratio; DCM, dichloromethane; DHAA, dehydroascorbic acid; DMF, *N*,*N*-dimethylformamide, DMP, Dess-Martin periodinane; DMSO, dimethyl sulfoxide; DTT, dithiothreitol; EtOAc, ethyl acetate; EtOH, ethyl alcohol; HPLC, high-performance liquid chromatography; IBX, 2-iodoxybenzoic acid; LCMS, liquid chromatography-mass spectrometry; MC-OSu, 2,5-dioxopyrrolidin-1-yl 6-(2,5-dioxo-2,5-dihydro-1H-pyrrol-1-yl)hexanoate; MeOH, methyl alcohol; MS, molecular sieves; MsCl, methanesulfonyl chloride; PAMPA, parallel artificial membrane permeability assay; PBD, pyrrolobenzodiazepine; SEC, size-exclusion chromatography; TBAF, tetra-*n*-butylammonium fluoride; TBAI, tetra-*n*-butylammonium iodide; TBSCl, *tert*-butyldimethylsilyl chloride; TFA, trifluoroacetic acid; THF, tetrahydrofuran; TLC, thin layer chromatography.

REFERENCES

1. Mantaj, J.; Jackson, P. J. M.; Rahman, K. M.; Thurston, D. E. From anthramycin to pyrrolobenzodiazepine (PBD)-containing antibody-drug conjugates (ADCs). *Angew. Chem. Int. Ed.* **2017**, *56*, 462-488.

2. Zheng, B.; Yu, S.-F.; del Rosario, G.; Leong, S. R.; Lee, G. Y.; Vij, R.; Chiu, C.; Liang, W.-C.; Wu, Y.; Chalouni, C.; Sadowsky, J.; Clark, V.; Hendricks, A.; Poon, K. A.; Chu, W.; Pillow, T.; Schutten, M. M.; Flygare, J.; Polson, A. G. An Anti-CLL-1 antibody-drug conjugate for the treatment of acute myeloid leukemia. *Clin. Cancer Res*. **2019**, *25*, 1358-1368.

3. Pillow, T. H.; Schutten, M.; Yu, S.-F.; Ohri, R.; Sadowsky, J.; Poon,K. A.; Solis, W.; Zhong, F.; Del Rosario, G.; Go, M. A. T.; Lau, J.; Yee, S.; He, J.; Liu, L.; Ng, C.; Xu, K.; Leipold, D. D.; Kamath, A. V.; Zhang, D.; Masterson, L.; Gregson, S. J.; Howard, P. W.; Fang, F.; Chen, J.; Gunzner-Toste, J.; Kozak, K. K.; Spencer, S.; Polakis, P.; Polson, A. G.; Flygare, J. A.; Junutula, J. R. Modulating therapeutic activity and toxicity of pyrrolobenzodiazepine antibody-drug conjugates with self-immolative disulfide linkers. *Mol. Cancer Ther*. **2017**, *16*, 871-878.

4. Saunders, L. R.; Bankovich, A. J.; Anderson, W. C.; Aujay, M. A.; Bheddah, S.; Black, K. A.; Desai, R.; Escarpe, P. A.; Hampl, J.; Laysang, A.; Liu, D.; Lopez-Molina, J.; Milton, M.; Park, A.; Pysz, M. A.; Shao, H.; Slingerland, B.; Torgov, M.; Williams, S. A.; Foord, O.; Howard, P.; Jassem, J.; Badzio, A.; Czapiewski, P.; Harpole, D. H.; Dowlati, A.; Massion, P. P.; Travis, W. D.; Pietanza, M. C.; Poirier, J. T.; Rudin, C. M.; Stull, R. A.; Dylla. S. J. A DLL3-targeted

antibody-drug conjugate eradicates high-grade pulmonary neuroendocrine tumor-initiating cells *in vivo*. *Science Trans. Med*. **2015**, *7*, 302ra136.

5. Sutherland, M. S. K.; Walter, R. B.; Jeffrey, S. C.; Burke, P. J.; Yu, C.; Kostner, H.; Stone, I.; Ryan, M. C.; Sussman, D.; Lyon, R. P.; Zeng, W.; Harrington, K. H.; Klussman, K.; Westendorf, L.; Meyer, D.; Bernstein, I. D.; Senter, P. D.; Benjamin, D. R.; Drachman, J. G.; McEarchern, J. A. SGN-CD33A: a novel CD33-targeting antibody-drug conjugate using a pyrrolobenzodiazepine dimer is active in models of drug-resistant AML. *Blood* **2013**, *122*, 1455-1463.

6. Caimi, P.; Kahl, B. S.; Hamadani, M.; Carlo-Stella, C.; He, S.; Ungar, D.; Feingold, J.; Ardeshna, K. M.; Radford, J.; Solh, M.; Heffner, L.; O'Connor, O. A. Safety and efficacy of ADCT-402 (loncastuximab tesirine), a novel antibody drug conjugate, in relapsed/refractory follicular lymphoma and mantle cell lymphoma: Interim results from the phase 1 first-in-human study. *Blood* **2018**, *132*, Suppl 1, 2874.

7. (a) Zammarchi, F.; Havenith, K.; Chivers, S.; Hogg, P. W.; Britten, C.; Dissanayake, S.; Tyrer, P.; Bertelli, F.; Hutchinson, I.; Masterson, L.; Howard, P.; Hartley, J. A.; van Berkel, P. H. Preclinical activity of ADCT-601, a novel pyrrolobenzodiazepine (PBD) dimer-based antibody-drug conjugate (ADC) targeting AXL-expressing tumors. *Cancer Res*. **2018**, *78* (13 Suppl), Abstract 2792A. (b) ADC Therapeutics press release, January 16, 2019; https://www.globenewswire.com/news-release/2019/01/16/1696491/0/en/ADC-Therapeutics-

Announces-First-Patient-Dosed-in-Phase-I-Clinical-Trial-of-ADCT-601-in-Advanced-Solid-Tumors.html (accessed July 7, 2020).

8. (a) Kinneer, K.; Meekin, J.; Varkey, R.; Xiao, X.; Zhong, H.; Breen, S.; Hurt, E.; Thomas, S.; Flynn, M.; Hynes, P.; Bezabeh, B.; Chen, C.; Wetzel, L.; Chen, R.; Tai, Y.-T.; Anderson, K. C.; Herbst, R.; Tice, D. Preclinical evaluation of MEDI2228, a BCMA-targeting pyrrolobenzodiazepine-linked antibody drug conjugate for the treatment of multiple myeloma. *Blood* **2017**, *130*, Suppl 1, 3153. (b) ClinicalTrials.gov, NCT03489525 (accessed July 7, 2020).

9. (a) Flynn, M. J.; Zammarchi, F.; Tyrer, P. C.; Akarca, A. U.; Janghra, N.; Britten, C. E.; Havenith, C. E. G.; Levy, J.-N.; Tiberghien, A.; Masterson, L. A.; Barry, C.; D'Hooge, F.; Marafioti, T.; Parren, P. W. H. I.; Williams, D. G.; Howard, P. W.; van Berkel, P. H.; Hartley. J. A. ADCT-301, a pyrrolobenzodiazepine (PBD) dimer-containing antibody-drug conjugate (ADC) Targeting CD25-expressing hematological malignancies. *Mol. Cancer Ther*. **2016**, *15*, 2709-2721. (b) Hamadani, M.; Collins, G. P.; Samaniego, F.; Spira, A. I.; Davies, A.; Radford, J.; Caimi, P.; Menne, T.; Boni, J.; Cruz, H.; Feingold, J.; He, S.; Wuerthner, J.; Horwitz, S. M. Phase 1 study of ADCT-301 (camidanlumab tesirine), a novel pyrrolobenzodiazepine-based antibody drug conjugate, in relapsed/refractory classical Hodgkin lymphoma. *Blood* **2018**, *132*, Suppl 1, 928.

10. Abbvie press release, August 29, 2019; https://news.abbvie.com/news/press-releases/abbvie-discontinues-rovalpituzumab-tesirine-rova-t-research-and-development-program.htm (accessed July 7, 2020).

11. Seattle Genetics press release, June 19, 2017; investor.seattlegenetics.com/news-releases/news-release-details/seattle-genetics-discontinues-phase-3-cascade-trial-vadastuximab (accessed July 7, 2020).

12. (a) Doronina, S. O.; Mendelsohn, B. A.; Bovee, T. D.; Cerveny, C. G.; Alley, S. C.; Meyer, D. L.; Oflazoglu, E.; Toki, B. E.; Sanderson, R. J.; Zabinski, R. F.; Wahl, A. F.; Senter, P. D. Enhanced activity of monomethylauristatin F through monoclonal antibody delivery: Effects of linker technology on efficacy and toxicity. *Bioconjugate Chem*. **2006**, *17*, 114-124. (b) Maderna, A.; Leverett, C. A. Recent advances in the development of new auristatins: Structural modifications and application in antibody drug conjugates. *Mol. Pharmaceutics* **2015**, *12*, 1798-1812. (c) Li, F.; Emmerton, K. K.; Jonas, M.; Zhang, X.; Miyamoto, J. B.; Setter, J. R.; Nicholas, N. D.; Okeley, N. M.; Lyon, R. P.; Benjamin, D. R.; Law, C.-L. Intracellular released payload influences potency and bystander-killing effects of antibody-drug conjugates in preclinical models. *Cancer Res*. **2016**, *76*, 2710-2719. (d) Hingorani, D. V.; Doan, M. K.; Camargo, M. F.; Aguilera, J.; Song, S. M.; Pizzo, D.; Scanderbeg, D. J.; Cohen, E. E. W.; Lowy, A. M.; Adams, S. R.; Advani, S. J. Precision chemoradiotherapy for HER2 tumors using antibody conjugates of an auristatin derivative with reduced cell permeability. *Mol. Cancer Ther*. **2020**, *19*, 157-167.

13. (a) Widdison, W. C.; Ponte, J. F.; Coccia, J. A.; Lanieri, L.; Setiady, Y.; Dong, L.; Skaletskaya, A.; Hong, E. E.; Wu, R.; Qiu, Q.; Singh, R.; Salomon, P.; Fishkin, N.; Harris, L.; Maloney, E. K.; Kovtun, Y.; Veale, K.; Wilhelm, S. D.; Audette, C. A.; Costoplus, J. A.; Chari,

R. V. J. Development of anilino-maytansinoid ADCs that efficiently release cytotoxic metabolites in cancer cells and induce high levels of bystander killing. *Bioconjugate Chem*. **2015**, *26*, 2261-2278. (b) Costoplus, J. A.; Veale, K. H.; Qiu, Q.; Ponte, J. F.; Lanieri, L.; Setiady, Y.; Dong, L.; Skaletskaya, A.; Bartle, L. M.; Salomon, P.; Wu, R.; Maloney, E. K.; Kovtun, Y. V.; Ab, O.; Lai, K.; Chari, R. V. J.; Widdison, W. C. Peptide-cleavable self-immolative maytansinoid antibody-drug conjugates designed to provide improved bystander killing. *ACS Med. Chem. Lett*. **2019**, *10*, 1393-1399.

14. Ogitani, Y.; Hagihara, K.; Oitate, M.; Naito, H.; Agatsuma, T. Bystander killing effect of DS-8201a, a novel anti-human epidermal growth factor receptor 2 antibody-drug conjugate, in tumors with human epidermal growth factor receptor 2 heterogeneity. *Cancer Sci*. **2016**, *107*, 1039-1046.

15. For a related example that accomplishes indolinobenzodiazepine ADC payload modification via an attached linker, see: Reid, E. E.; Archer, K. E.; Shizuka, M.; Wilhelm, A.; C. Yoder, N. C.; Bai, C.; Fishkin, N. E.; Harris, L. Maloney, E. K.; Salomon, P.; Hong, E.; Wu, R.; Ab, O.; Jin, S.; Lai, K. C.; Sikka, S.; Chari, R. V. J.; Miller. M. L. Effect of linker stereochemistry on the activity of indolinobenzodiazepine containing antibody-drug conjugates (ADCs). *ACS Med. Chem. Lett*. **2019**, *10*, 1193-1197.

16. (a) Cailleau, T.; Adams, L. R.; Arora, N.; Kang, G.-D.; Masterson, L.; Patel, N.; Hartley, J. A.; Mao, S.; Harper, J.; Howard, P. W. Potentiation of PBD dimers by lipophilicity manipulation. *Curr. Top. Med. Chem*. **2019**, *19*, 741-752. (b) Kinneer, K.; Meekin, J.;

Tiberghien, A. C.; Tai, Y.-T.; Phipps, S.; Kiefer, C. M.; Rebelatto, M. C.; Dimasi, N.; Moriarty, A.; Papadopoulos, K. P.; Sridhar, S.; Gregson, S. J.; Wick, M. J.; Masterson, L.; Anderson, K. C.; Herbst, R.; Howard, P. W.; Tice. D. A. SLC46A3 as a potential predictive biomarker for antibody-drug conjugates bearing noncleavable linked maytansinoid and pyrrolobenzodiazepine warheads. *Clin. Cancer Res*. **2018**, *24*, 6570-6582.

17. (a) Smellie, M.; Bose, D. S.; Thompson, A. S.; Jenkins, T. C.; Hartley, J. A.; Thurston, D. E. Sequence-selective recognition of duplex DNA through covalent interstrand cross-linking: Kinetic and molecular modeling studies with pyrrolobenzodiazepine dimers. *Biochemistry* **2003**, *42*, 8232-8239. (b) Gregson, S. J.; Howard, P. W.; Gullick, D. R.; Hamaguchi, A.; Corcoran, K. E.; Brooks, N. A.; Hartley, J. A.; Jenkins, T. C.; Patel, S.; Guille, M. J.; Thurston, D. E. Linker length modulates DNA cross-linking reactivity and cytotoxic potency of C8/C8' ether-linked C2-exo-unsaturated pyrrolo[2,1-*c*][1,4]benzodiazepine(PBD) dimers. *J. Med. Chem*. **2004**, *47*, 1161-1174.

18. Gregson, S. J.; Masterson, L. A.; Wei, B.; Pillow, T. H.; Spencer, S. D.; Kang, G.-D.; Yu, S.-F.; Raab, H.; Lau, J.; Li, G.; Phillips, G. D. L.; Gunzner-Toste, J.; Safina, B. S.; Ohri, R.; Darwish, M.; Kozak, K. R.; dela Cruz-Chuh, J.; Polson, A.; Flygare, J. A.; Howard, P. W. Pyrrolobenzodiazepine dimer antibody-drug conjugates: Synthesis and evaluation of noncleavable drug-linkers. *J. Med. Chem.* **2017**, *60*, 9490-9507.

19. Zhang, D.; Pillow, T. H.; Ma, Y.; Cruz-Chuh, J.; Kozak, K. R.; Sadowsky, J. D.; Phillips, G. D. L.; Guo, J.; Darwish, M.; Fan, P.; Chen, J.; He, C.; Wang, T.; Yao, H.; Xu, Z.; Chen, J.; Wai,

J.; Pei, Z.; Hop, C. E. C. A.; Khojasteh, S. C.; Dragovich, P. S. Linker immolation determines cell killing activity of disulfide-linked pyrrolobenzodiazepine antibody-drug conjugates. *ACS Med. Chem. Lett.* **2016**, *7*, 988-993.

20. Kansy, M.; Senner, F.; Gubernator, K. Physicochemical high throughput screening: Parallel artificial membrane permeation assay in the description of passive absorption processes. *J. Med. Chem.* **1998**, *41*, 1007-1010.

21. Dubowchik, G. M.; Firestone, R. A. Cathepsin B-sensitive dipeptide prodrugs. 1. A model study of structural requirements for efficient release of doxorubicin. *Bioorg. Med. Chem. Lett*. **1998**, *8*, 3341-3346.

22. (a) Gregson, S. J.; Barrett, A. M.; Patel, N. V.; Kang, G.-D.; Schiavone, D.; Sult, E.; Barry, C. S.; Vijayakrishnan, B.; Adams, L. R.; Masterson, L. A.; D'Hooge, F.; Snaith, M.; Harper, J.; Hartley, J. A.; Howard, P. W. Synthesis and evaluation of pyrrolobenzodiazepine dimer antibody-drug conjugates with dual β-glucuronide and dipeptide triggers. *Eur. J. Med. Chem*. **2019**, *179*, 591-607. (b) Jiang, Y.-P.; Liu, B. Y.; Zheng, Q.; Panuganti, S.; Chen, R.; Zhu, J.; Mishra, M.; Huang, J.; Dao-Pick, T.; Roy, S.; Zhao, X.-X.; Lin, J.; Banik, G.; Hsi, E. D.; Mandalam, R.; Junutula, J. R. CLT030, a leukemic stem cell-targeting CLL1 antibody-drug conjugate for treatment of acute myeloid leukemia. *Blood Adv*. **2018**, *2*, 1738-1749.

23. The mAb nomenclature follows the EU convention described in: Edelman, G. M.; Cunningham, B. A.; Gall, W. E.; Gotlieb, P. D.; Rutishauser, U.; Waxdal, M. J. The covalent

structure of an entire γG immunoglobin molecule. *Proc. Natl. Acad. U.S.A*. **1969**, *63*, 78-85. For a comparison of the EU and the alternate Kabat mAb nomenclature systems, see table S1 in reference 24.

24. Ohri, R.; Bhakta, S.; Fourie-O'Donohue, A.; Dela Cruz-Chuh, J.; Tsai, S. P.; Cook, R.; Wei, B.; Ng, C.; Wong, A. W.; Bos, A. B.; Farahi, R.; Bhakta, J.; Pillow, T. H.; Raab, H.; Vandlen, R.; Polakis, P.; Liu, Y.; Erickson, H.; Junutula, J. R.; Kozak, K. R. High-throughput cysteine scanning to identify stable antibody conjugation sites for maleimide- and disulfide-based linkers. *Bioconjugate Chem*. **2018**, *29*, 473-485.

25. Loomis, K.; Smith, B.; Feng, Y.; Garg, H.; Yavlovich, A.; Campbell-Massa, R.; Dimitrov, D. S.; Blumenthal, R.; Xiao, X.; Puri, A. Specific targeting to B cells by lipid-based nanoparticles conjugated with a novel CD22-ScFv. *Exp. Mol. Path*. **2010**, *88*, 238-249.

26. (a) Shor, B.; Gerber, H.-P.; Sapra, P. Preclinical and clinical development of inotuzumab ozogamicin in hematological malignancies. *Mol. Immunol*. **2015**, *67*, 107-116. (b) Polson, A. G.; Calemine-Fenaux, J.; Chan, P.; Chang, W.; Christensen, E.; Clark, S.; de Sauvage, F. J.; Eaton, D.; Elkins, K.; Elliott, J. M.; Frantz, G.; Fuji, R. N.; Gray, A.; Harden, K.; Ingle, G. S.; Kljavin, N. M.; Koeppen, H.; Nelson, C.; Prabhu, S.; Raab, H.; Ross, S.; Slaga, D. S.; Stephan, J.-P.; Scales, S. J.; Spencer, S. D.; Vandlen, R.; Wranik, B.; Yu, S.-F.; Zheng, B.; Ebens, A. Antibody-drug conjugates for the treatment of non–Hodgkin's lymphoma: Target and linker-drug selection. *Cancer Res*. **2009**, *69*, 2358-2364.

27. (a) Rinnerthaler, G.; Gampenrieder, S. P.; Greil, R. HER2 directed antibody-drug-conjugates beyond T-DM1 in breast cancer. *Int. J. Mol. Sci*. **2019**, *20*, 1115. (b) Li, G.; Guo, J.; Shen, B.-Q.; Yadav, D. B.; Sliwkowski, M. X.; Crocker, L. M.; Lacap, J. A.; Phillips, G. D. L. Mechanisms of acquired resistance to trastuzumab emtansine in breast cancer cells. *Mol. Cancer Ther*. **2018**, *17*, 1441-1453. (c) Phillips, G. D. L.; Li, G.; Dugger, D. L.; Crocker, L. M.; Parsons, K. L.; Mai, E.; Blättler, W. A.; Lambert, J. M.; Chari, R. V. J.; Lutz, R. J.; Wong, W. L. T.; Jacobson, F. S.; Koeppen, H.; Schwall, R. H.; Kenkare-Mitra, S. R.; Spencer, S. D.; Sliwkowski, M. X. Targeting HER2-positive breast cancer with trastuzumab-DM1, an antibody-cytotoxic drug conjugate. *Cancer Res*. **2008**, *68*, 9280-9290.

28. Kinneer, K.; Meekin, J.; Tiberghien, A. C.; Tai, Y.-T.; Phipps, S.; Kiefer, C. M.; Rebelatto, M. C.; Dimasi, N.; Moriarty, A.; Papadopoulos, K. P.; Sridhar, S.; Gregson, S. J.; Wick, M. J.; Masterson, L.; Anderson, K. C.; Herbst, R.; Howard, P. W.; Tice, D. A. SLC46A3 as a potential predictive biomarker for antibody-drug conjugates bearing noncleavable linked maytansinoid and pyrrolobenzodiazepine warheads. *Clin. Cancer Res*. **2018**, *24*, 6570-6582.

29. Erickson, H. K.; Park, P. U.; Widdison, W. C.; Kovtun, Y. V.; Garrett, L. M.; Hoffman, K.; Lutz, R. J.; Goldmacher, V. S.; Blättler, W. A. Antibody-maytansinoid conjugates are activated in targeted cancer cells by lysosomal degradation and linker-dependent intracellular processing. *Cancer Res*. **2006**, *66*, 4426-4433.

30. (a) Gschwantler-Kaulich, D.; Grunt, T. W.; Muhr, D.; Wagner, R.; Kölbl, H.; Singer, C. F. HER specific TKIs exert their antineoplastic effects on breast cancer cell lines through the

involvement of STAT5 and JNK. *PLoS One*, **2016**, *11*, e0146311. (a) Pop, L. M.; Barman, S.; Shao, C.; Poe, J. C.; Venturi, G. M.; Shelton, J. M.; Pop, I. V.; Gerber, D. E.; Girard, L.; Liu, X.-y.; Behrens, C.; Rodriguez-Canales, J.; Liu, H.; Wistuba, I. I.; Richardson, J. A.; Minna, J. D.; Tedder, T. F.; Vitetta, E. S. A reevaluation of CD22 expression in human lung cancer. *Cancer Res*. **2014**, *74*, 263-271.

31. Smith, D. A.; Beaumont, K.; Maurer, T. S.; Di, L. Volume of distribution in drug design. *J. Med. Chem*. **2015**, *58*, 5691-5698.

32. Choi, J.; Vaidyanathan, G.; Koumarianou, E.; McDougald, D.; Pruszynski, M.; Osada, T.; Lahoutte, T.; Lyerly, H. K.; Zalutsky, M. R. *N*-Succinimidyl guanidinomethyl iodobenzoate protein radiohalogenation agents: Influence of isomeric substitution on radiolabeling and target cell residualization. *Nucl. Med. Biol*. **2014**, *41*, 802-812.

33. (a) Kanwal, I.; Mujahid, A.; Rasool, N.; Rizwan, K.; Malik, A.; Ahmad, G.; Shah, S. A. A.; Rashid, U.; Nasir, N. M. Palladium and copper catalyzed Sonogashira cross coupling an excellent methodology for C-C bond formation over 17 years: A review. *Catalysts* **2020**, *10*, 443. (b) Chinchilla, R.; Nájera, C. Recent advances in Sonogashira reactions. *Chem. Soc. Rev*. **2011**, *40*, 5084-5121.

34. Adhikari, P.; Zacharias, N.; Ohri, R.; Sadowsky, J. Site-specific conjugation to Cys-engineered THIOMAB™ antibodies. *Methods Mol. Biol*. **2020**, *2078*, 51-69.

35. Tohma, H.; Kita, Y. Hypervalent iodine reagents for the oxidation of alcohols and their application to complex molecule synthesis. *Adv. Synth. Catal*. **2004**, *346*, 111-124.

36. For alternate preparations of dibromide **46** see: (a) Duchêne, K.-H.; Vögtle, F. A hydrocarbon skeleton with twelve identical functional groups. Synthesis of a dodeca host compound. *Synthesis* **1986**, 659-661. (b) Dash, B. P.; Satapathy, R.; Gaillard, E. R.; Maguire, J. A.; Hosmane, N. S. Synthesis and properties of carborane-appended C3-symmetrical extended π systems. *J. Am. Chem. Soc*. **2010**, *132*, 6578-6587. (c) Sookcharoenpinyo, B.; Klein, E.; Ferrand, Y.; Walker, D. B.; Brotherhood, P. R.; Ke, C.; Crump, M. P.; Davis, A. P. High-affinity disaccharide binding by tricyclic synthetic lectins. *Angew. Chem. Int. Ed*. **2012**, *51*, 4586-4590.

37. Dragovich, P.; Pei, Z.; Pillow, T.; Sadowsky, J.; Verma, V.; Zhang, D. Pyrrolobenzodiazepine prodrugs and antibody conjugates thereof. International patent application, **2018**, WO 201831662.

38. Rettig, M.; Weingarth, M.; Langel, W.; Kamal, A.; Kumar, P. P.; Weisz, K. Solution structure of a covalently bound pyrrolo[2,1-c][1,4]benzodiazepinebenzimidazole hybrid to a 10mer DNA duplex. *Biochemistry* **2009**, *48*, 12223-12232.

Table of Contents Graphic: